The Weddell Gyre heat budget associated with the Warm Deep Water circulation derived from Argo Floats

Krissy Anne Reeve[1], Torsten Kanzow[1,2], Olaf Boebel[1], Myriel Vredenborg[1], Volker Strass[1], Rüdiger Gerdes[1,3]

5   [1]Alfred Wegener Institute, Bremerhaven, Germany

[2]Bremen University, Department of Physics and Electrical Engineering, Bremen, Germany

[3]Jacobs University, Bremen, Germany

Correspondence: Krissy Anne Reeve (krissy.reeve@awi.de)

Abstract: The Weddell Gyre plays an important role in the global climate system by supplying heat to underneath the ice shelves, and to the formation of deep and bottom water masses, which have been subject to widespread warming over past decades. In this study, we investigate the redistribution of heat throughout the Weddell Gyre by diagnosing the terms of the heat conservation equation for a 1000 m thick layer of water encompassing the core of Warm Deep Water. The spatial distribution of the different advective and diffusive terms in terms of heat tendencies are estimated using gridded climatologies of temperature and velocity, obtained from Argo floats in the Weddell Gyre from 2002 to 2016. While the results are somewhat noisy on the grid scale, the heat budget (i.e., the sum of all terms) nearly closes when integrated over the southern limb and the interior circulation cell of the Weddell Gyre. There is an overall balance between the mean horizontal advection and horizontal turbulent diffusion of heat, whereas the vertical terms contribute comparatively little to the heat budget. Heat convergence due to mean horizontal advection balances with divergence due to horizontal turbulent diffusion in the southern limb of the Weddell Gyre. In contrast, heat divergence due to mean horizontal advection nearly balances with convergence due to horizontal turbulent diffusion in the interior circulation cell of the Weddell Gyre. Heat is advected into the Weddell Gyre along the southern limb, some of which is turbulently diffused northwards into the interior circulation cell, while some is turbulently diffused southwards towards the shelf seas. This suggests that horizontal turbulent diffusion plays a role in transporting heat both towards the gyre interior where upwelling occurs, as well as towards the ice shelves. Horizontal turbulent diffusion is also a mechanism by which heat can be transported into the Weddell Gyre across the open northern boundary.

Plain Language Summary: Ocean currents in the Weddell Sea are governed by a cyclonic gyre circulation, which is connected to the Atlantic sector of the circumpolar Southern Ocean to its north. Cyclonic means that the horizontal circulation is clockwise, and deep waters are brought close to the surface in the centre by upwelling. The eastern limb of this cyclonic gyre transports relatively warm water poleward, where it loses heat to the atmosphere and by contact with the ice shelves. Thereby the water becomes denser, as also by salty brine released during the freezing of sea ice. The densest water masses then sink down the Antarctic continental slope, and after northward transport with western limb of the gyre fill the deepest basins of abyssal global ocean. The main source water mass for these processes and also the main source of heat to the Weddell Sea is the so-called Warm Deep Water. Previous studies have shown the whole water column, especially in the deeper layers, is warming over recent decades in the Weddell Sea. Warm Deep Water, however, varies in its properties too strongly to tease out long-term trends. To better understand how Warm Deep Water redistributes heat throughout the Weddell Gyre, we use hydrography and drift velocity observations from a fleet of Argo floats freely drifting throughout the Weddell Gyre between 2002 and 2016. We estimate a heat budget in a 1000 m thick layer, where the upper boundary is defined as the mid-thermocline, which varies typically around 150 m. Thus, we ensure that the core of Warm Deep Water, characterised by a sub-surface temperature maximum, is always included in the 1000 m-thick layer, regardless of its vertical position in the water column. Overall, large uncertainty and variability prevents us from interpreting the results on a local scale, but interesting features emerge when integrating the heat budget over large areas. According to our results heat is advected into the westward-flowing

southern limb from the east, but also upwards from below the layer throughout the whole gyre. Turbulent diffusion removes heat from the Warm Deep Water core through the top of the layer throughout (i.e., upwards through the thermocline into the upper ocean), and also transports heat from the southern limb, into the interior of the gyre where Warm Deep Water recirculates and moves closer to the surface, as well as southwards towards the Antarctic coastline. Lastly, turbulent diffusion also brings heat into the gyre across the northern boundary.

1 Introduction

Understanding the drivers and pathways of large-scale ocean circulation is a fundamental component of climate science (Rhein et al., 2013). To comprehend the regulatory role of the oceans in the climate system, one can determine the ocean heat budget, which describes the redistribution of heat throughout the ocean by means of horizontal and vertical advection, turbulent diffusion, and surface heat fluxes to the atmosphere (e.g., Tamsitt et al., 2016; an adapted form of the heat budget equation is given in Eq. 1.1).

The Weddell Gyre is located south of 50° S in the Atlantic sector of the Southern Ocean, where Circumpolar Deep Water (CDW) predominantly enters the gyre's southern limb in the east at about 30° E. The CDW that enters the Weddell Gyre is commonly referred to as Warm Deep Water (WDW). WDW circulates the cyclonic gyre, undergoing cooling and freshening on-route, through interaction with the underlying and overlying water masses (e.g., Fahrbach et al., 2004; Klatt et al., 2005; Fahrbach et al., 2011; Leach et al., 2011). The core of WDW is identified as the sub-surface temperature maximum (hereon referred to as Θ_{max}), which feeds heat into the Weddell Gyre (Fahrbach et al., 2004, 2011; Cisewski et al., 2011; Ryan et al., 2016). The distribution of temperature at the depth of the Θ_{max} is shown in Fig. 1, which is derived from in situ observations from Argo floats (from Reeve et al., 2016, 2019). The Weddell Gyre has been ascribed the role of a heat buffer (Fahrbach et al., 2011), in that it acts to store and redistribute heat and salt in the water column, effectively transferring heat to the deeper layers where it is ultimately exported northwards, spreading throughout the abyssal global ocean (e.g., Foster et al., 1987; Naveira Garabato et al., 2002, 2016; Fahrbach et al., 2011).

Warming trends over recent decades have been observed in the WSDW and WSBW (Weddell Sea –Deep and -Bottom Water respectively) (Fahrbach et al., 2011; Meredith et al., 2011; Strass et al., 2020). However, their primary source of heat, WDW, exhibits pronounced decadal variations and shows no significant long-term warming trend (Fahrbach et al., 2011; Kerr et al., 2017). While Strass et al. (2020) show that the whole water column below 700 m exhibits a significant long-term warming trend, which would incorporate the lower part of the WDW layer, they also observed significant variability and even areas of cooling in the upper 700 m, which incorporates a significant chunk of the WDW layer.

In this study, we combine observations of the velocity field (Reeve et al., 2019) with the temperature field (Reeve et al., 2016), both derived primarily from Argo floats, to diagnose components of the heat budget of a fixed volume of water fully encompassing the core of WDW within the Weddell Gyre. Given the near-surface seasonal cycle is unresolved throughout, a full basin analysis of the upper 50 m is unfeasible. By analysing the heat budget for a fixed volume encompassing the core of WDW, we can, however, determine the ways in which heat from WDW is redistributed throughout the Weddell Gyre. The rest of this paper is structured as follows. Section 2 describes the data sources used in this study, while Section 3 details the method of applying the heat budget, and its associated estimation of uncertainty. Section 4 presents the individual heat budget terms for the Weddell Gyre for the whole region as well as integrated over specific areas, while Section 5 interprets these results in context of the study limitations and the literature. Lastly, Section 6 provides our final summary.
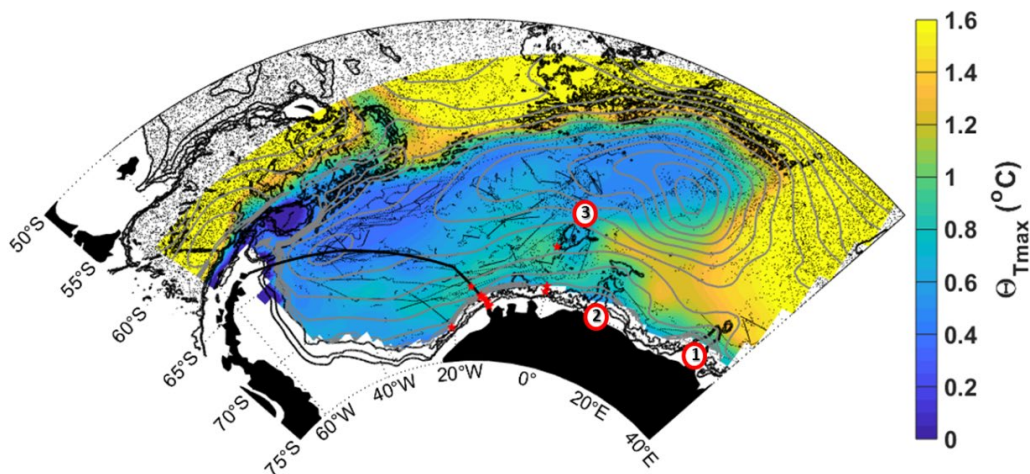
Figure 1: Sub-surface conservative temperature at the depth of temperature maximum (Θ_{max}) with streamlines (grey contours) of the vertically integrated stream function for 50-2000 dbar with a spacing of 5 Sv, derived from in-situ observations from Argo floats (Reeve et al., 2019, 2016). Black dots show Argo float profile positions and red stars show mooring positions used in velocity field estimates. The thick black line shows the repeat ship-based transect from Kapp Norvegia to Joineville Island. The red circles labelled 1-3 show Gunnerus Ridge, Astrid Ridge and Maud Rise, respectively. The black contours show the 1000, 2000 and 3000 m isobaths, from the general bathymetric chart of the oceans (GEBCO, IOC et al., 2003).

2 Data sources

80   For this study we computed the heat budget of the entire Weddell Gyre using different sets of data from various sources, which will be described in more detail in the following subsections.

2.1 Data sources

Table 1 describes the data sources used for determining the heat budget presented in this paper. Each source is then described in further detail in Sections 2 and 3, as well as in the Supplement (S1-4).

Table 1. A summary of the associated data source, method and citation for each variable required in the heat budget (Eq. 1.2 in Section 3, and column 2 below).

Section for details	Variable	Data source	Methodology	Citation
2.2	Gridded Temperature (θ)	Argo floats (2002-2016)	Objective mapping	Reeve et al., 2016
2.2	Gridded horizontal velocity (U)	Argo floats (2002-2016)	Objective mapping, cost function	Reeve et al., 2019
2.2	Long-term mean velocity at the shelf edge (U)	Moorings (1989-2016)		Le Piah et al., 2020
2.2	Bathymetry	GEBCO		IOC et al., 2003
S3	Vertical (Ekman) velocity (w_E)	ERA5-interim reanalysis and Polar Pathfinder (listed below)	Regridded using a distance-weighted mean	Hersbach et al., (2020) & Tschudi et al., (2019)
S3	Wind stress ($\tau_{air\text{-}ocean}$) derived from wind field at 10 m above sea surface (U_{10})	ERA5-interim reanalysis	Used to compute w_E	Hersbach et al., (2020)
S3	Sea-ice concentration (α)	ERA5-interim reanalysis	Used to compute w_E	Hersbach et al., (2020)

S3	Sea-ice velocity (U_{ice})	Polar Pathfinder Daily 25 km EASE-Grid Sea Ice Motion Vectors	Used to compute w_E	Tschudi et al., (2019)
3 & S4	Horizontal diffusivity (κ_H)	Sevellec et al., (2022), and estimates in the literature (see citation)	Where available (i.e., outskirts of gyre) the Sevellec dataset. Infilled within gyre with a constant value based on the literature	Sevellec et al., 2022; Donnelly et al. (2017); Zika et al. (2009) & Cole et al., (2015)
3	Vertical diffusivity (κ_V)	Based on estimates in the literature (see citation)		Donnelly et al. (2017), Zika et al. (2009) & Cole et al., (2015)
S2	Air-sea heat fluxes	ERA-interim reanalysis		Jones et al., 2016

85

2.2   Gridded velocity and temperature fields derived from Argo floats:

All Argo float data available for the Weddell Gyre region between 2002 and 2016 were used in this study to create gridded fields of velocity and conservative temperature. The latter was derived using the TEOS-10 program in MATLAB (McDougall et al., 2011). We applied objective mapping to the profile data resulting in a climatology of gridded conservative temperature on 41 pressure levels between 50 and 2000 dbar. The grid cell resolution varies slightly with changing latitude (Reeve et al.

90   2019), but is on the order of ~80 x 60 km. This method follows, and is an extension of the objective mapping provided in Reeve et al. (2016), and the reader is referred to that study for further details on the data quality control and mapping method used in this study. The absolute velocity field was derived from Argo float trajectory data at the depth of the float drift (800 dbar in the Weddell Gyre). This process required careful quality control assessments and surface drift corrections following

95   Park et al. (2005), and, given that under-ice profiles have no geo-located position, all such interpolated trajectories were omitted from the study. Thus, the derived velocity field exhibits considerable bias to summer conditions. The velocities were objectively mapped to provide a grid of absolute velocity at 800 dbar. This process is detailed in Reeve et al. (2019).

Following Reeve et al. (2019), a stream function was fitted to the velocity field at 800 dbar through the application of a cost function. By applying a cost function, the resulting stream function provides a best fit for the entire Weddell Gyre, where the

100   direction of mean flow at the boundaries are assumed to be parallel to the boundaries. . The stream function at 800 dbar provides the reference level for the relative geostrophic velocity, derived from the gridded density field from Reeve et al. (2016), above. For full details on this methodology, refer to Reeve et al. (2019), which, in addition to Reeve et al. 2016, is the prelude to this study. In Reeve et al. (2019), a careful error analysis and a detailed comparison of volume transports to available estimates in the literature justify the method as a reasonable solution to obtaining a large-scale observation-based estimate of

105   the Weddell Gyre circulation.

There are, however, important improvements between the stream function provided in Reeve et al. (2019), and the stream function used in this study. The cost function was adapted to allow for a variable coastline, so that the stream function provides a solution which includes the southern ice shelf edge east of the Prime Meridian (though not the shelf edge currents, such as the Antarctic Slope Front, which are not resolved in this study as they are beyond the domain of the Argo floats), which is

110   excluded in Reeve et al. (2019). To better estimate the velocity field along the southern coast of the Weddell Gyre, a few minor adjustments were made to the gridded velocity field prior to fitting a stream function. Firstly, long-term average velocities derived from mooring data were included at the coast near the Prime Meridian and Kapp Norvegia, to better resolve the flow which follows the coastline as it curves southwards towards the Filchner-Ronne ice shelves (the mooring positions are marked in Fig. 1. See Le Piah et al. 2020 for further information about the mooring data). Secondly, the velocity field at Gunnerus

115   Ridge (also marked in Fig. 1) required special treatment. The trajectories of Argo floats show a tight, bathymetrically steered flow around Gunnerus Ridge, which is lost during the objective mapping process due to larger length scales. Also, while the potential vorticity values to either side of the ridge are the same, the direction of the flow is opposing (i.e., primarily northwards on the eastern flank of Gunnerus Ridge and southwards to the west of Gunnerus Ridge; see Fig. 11 in Reeve et al. 2019). This

opposing direction is averaged out in the objective mapping. Therefore, after the objective mapping, the closest grid cells to
Gunnerus Ridge are replaced with direct velocity measurements derived from the three Argo floats that drift along the ridge
(the Argo floats have WMO numbers: 7900164, 7900166 and 7900168). There are caveats to this decision, in that these are
data points from three floats with a limited time span (from February-May 2007, and then December 2007 until April 2008),
during a period when the area is ice-free. However, by making this adjustment, we improve the performance of the cost function
in providing a stream function representative of the large-scale circulation, which includes a more complete inflow (in
comparison to Fig. 4 in Reeve et al. 2019). The resulting stream function for the vertically integrated flow from 50-2000 dbar
is shown in Fig. 1, where the streamlines curve around Gunnerus Ridge, indicating the main inflow into the southern limb of
the Weddell Gyre.

3   Methods

3.1   The heat budget

Due to conservation, the heat storage of a certain ocean volume needs to equal the sum of all fluxes comprising advection and
turbulent diffusion, both vertical and horizontal. Thus, the heat budget integrated for a volume of water not in contact with the
atmosphere is defined as:

$$\frac{d\theta}{dt} = -\nabla_H (U \cdot \theta) - w_E \frac{d\theta}{dz} + \kappa_H \nabla_H^2 \theta + \kappa_V \frac{d^2\theta}{dz^2} \tag{1.1}$$

$$\rho_0 C_p \int_{mT-1000}^{mT} \frac{d\theta}{dt} dz = \rho_0 C_p \left\{ \int_{mT-1000}^{mT} (-\nabla_H (U \cdot \theta) + \kappa_H \nabla_H^2 \theta)\, dz - w_E (\theta_{mT} - \theta_{mT-1000}) + \kappa_V \left(\frac{\partial\theta}{\partial z}\Big|_{mT} - \frac{\partial\theta}{\partial z}\Big|_{mT-1000} \right) \right\} \tag{1.2}$$

where ∇_H is the horizontal divergence operator, U is the horizontal geostrophic velocity, θ is the conservative temperature, w_E
is the vertical velocity (defined as the Ekman pumping velocity; see Supplements S3), z is depth and κ_H and κ_V are the
horizontal and vertical diffusivity respectively (adapted from Tamsitt et al. 2016). For the vertical integration in Eq. 1.2, the
subscript m_T describes the mid-point of the thermocline, which provides the upper boundary, while $m_T +1000$ describes the
lower boundary (explanation of the vertical boundaries is provided in the Supplements S1). Each term is multiplied by the
specific heat capacity of seawater, C_p (~4000 J K^{-1} Kg^{-1}), and seawater density, (ρ_0 = 1027 kg m^{-3}), and integrated for a 1000
m thick layer so that units of each component are given in W m^{-2}. The first term on the right-hand side in Eq. 1.1 describes the
mean horizontal geostrophic heat advection, where U is derived from horizontal differentiation of the geostrophic stream
function derived from Argo float data (i.e., where u = $\partial\psi/\partial y$ and v = $-\partial\psi/\partial x$; see Section 2.2 and Reeve et al. 2019). Since
we derive velocity from a non-divergent stream function, we assume geostrophic flow conditions and omit ageostrophic
advection from the first term. This is a pertinent assumption given that the Ekman Layer is excluded from the analysis. The
second term on the right-hand side in Eq. 1.1 describes the mean vertical heat advection. The third and fourth terms in Eq. 1.1
(or, the second part of the first term and the third term in Eq. 1.2) describe the horizontal and vertical turbulent heat diffusion
components respectively. The sum of these terms results in an estimate of heat tendency over time (dθ/dt), which can be used
to determine mean temperature change for a column of water, although this method results in an accumulation of associated
errors of the individual terms, and should therefore be treated with caution. Maps of the different components are provided in
the results section.

There are two unknowns in Eq. 1. These are the horizontal and vertical diffusivities, κ_H and κ_V respectively. For the northern
and eastern outskirts of the Weddell Gyre, we define κ_H from the dataset provided by Sevellec et al. (2022). For the rest of the
Weddell Gyre, we define κ_H as 400 ± 200 m^{2}s^{-1}, based on the varying values provided in the literature (See Supplements S4
for our reasoning and maps of κ_H). We define κ_V as 2.6 x 10^{-5} ± 2.4x10^{-5} m^{2}s^{-1}, again based on values provided in the literature.
The error ranges are to provide a range of reasonable estimates while acknowledging lack of consensus of appropriate values

155   for the diffusivities. While κ_v is similar to Donnelly et al.'s estimate of 2.4 x 10^{-5} m^2 s^{-1}, our baseline horizontal diffusivity is slightly larger than the 247 m^2 s^{-1} provided by Donnelly et al. (2017; though within range of our values provided by the uncertainty range) and is chosen in consideration of a range of values provided by Donnelly et al. (2017), Zika et al. (2009) and Cole et al. (2015), of 247 m^2 s^{-1}, 300 m^2 s^{-1} and 200-2000 m^2 s^{-1} respectively. Our chosen baseline κ_H is larger than the first two listed here and more closely aligned with Cole et al. (2015), because we focus on larger length-scales, most similar

160   to the latter study, owing to the resolution and sample density of our data set. The implications of these decisions are discussed in Section 5.

3.2   Assessing the uncertainty

The errors for each heat budget term are calculated using the laws of propagation, as detailed in the Supplement to this paper (S7). The main sources of error are from the variables: temperature, horizontal velocity, vertical (Ekman) velocity, and

165   unknown diffusivity, which is assumed constant in the horizontal for the Weddell Gyre interior and southern limb, and throughout the whole Weddell Sea in the vertical.

We used the objective mapping error to represent the error for temperature (Fig. S7), which is provided in Reeve et al. (2016), and assumed to be the dominating source of error for temperature. This means that the error is also representative of the length scales applied in the objective mapping (Reeve et al., 2016). In Reeve et al. (2016), the length scales were assigned based on

170   an investigation which showed that 95 % of the grid points have at least 40 Argo profiles within a distance of 500 km (we were then able to reduce this to 400 km in Reeve et al. 2019), which was thus the length scale applied in the second stage of the objective mapping, along with a fractional scale on the effect of f/H, which alters the shape of the area of influence about a grid point from circular, when the bottom bathymetry is flat, to elongated, when a grid point is in close proximity to bathymetric gradients (Reeve et al. 2016). Since the focus is a climatological mean from 2002 to 2016, the applied length

175   scales are chosen for the mapping to represent the large-scale field of the entire Weddell Gyre (Reeve et al., 2016). The resulting mapping errors are large in regions where bathymetry is complex and data coverage is sparse, and low in regions where the bathymetry is flat or where data density is high. Thus, the regions of largest uncertainty include the northern periphery of the gyre, where data is relatively abundant but the bathymetry is complex, and the eastern edge of the Weddell Gyre, where data is sparse (Fig. S7).

180   The error for horizontal velocity was provided in Reeve et al. (2019), and is derived from the stream function, where a sensitivity study was implemented, perturbing the velocity field using a combination of factors (mapping errors and drift correction), to provide a range of possible stream function values, from which a standard error was estimated.

Since uncertainty is currently unavailable for the ERA-5 reanalysis data that provided the wind stress field from which Ekman vertical velocity was computed, we took the standard error of the mean of a monthly time series from January 2002 to

185   December 2016 to represent the error for vertical velocity. This represents the natural temporal variability of the vertical velocity, which we assume to be dominating over other possible sources of error, given the large seasonal variability of the wind field.

Lastly, we arbitrarily define an uncertainty range for the diffusivity terms, to be $\pm$ 200 m^{2}s^{-1} and 2.4x10^{-5} m^{2}s^{-1} for the horizontal and vertical diffusivity terms respectively (with the exception of the regions where the Sevellec et al. (2022) dataset is used,

190   where a standard error of the mean is used, see Supplements S4). These are large ranges to account for the possible range in values available in the literature, while acknowledging the lack of consensus and reliable data for this input (we discuss this further in Section 5.1.3). The derivation for the propagated errors is provided in the Supplement (S7), along with maps of the error for each heat budget term. The errors are provided in the large-scale integrations of the IC and SL in Figs. 3-7 (as pale blocks of colour surrounding the lines).

195

4   Results

Each of the maps provided throughout this paper show streamlines (grey contours) indicating the horizontal circulation of the Weddell Gyre derived from Argo floats (see Section 2.2 and Reeve et al. 2019 for further details). Where the streamlines are closely spaced, flow is more intense than where they are loosely spaced. The streamlines describe a double-gyre structure

200   whereby the western sub-gyre is weaker than the elongated, stronger eastern sub-gyre. The following section is presented in two parts. In part one, we provide maps of the vertically integrated heat budget terms (from Eq. 1.2), to obtain an overview of the large-scale heat field of the Weddell Gyre. In part 2, we consider the zonal variation of the heat budget, for two regions: (1) the southern limb (SL), which describes the westward flowing part of the gyre that extends from Gunnerus Ridge (~33°E) to ~45°W (i.e., where the stream function, ψ, is 16 to 30 Sv; the stippled area in Fig. 2b) and (2) the interior circulation cell

205   (IC), where streamlines form a fully closed circuit west of Gunnerus Ridge, incorporating both the eastern and western sub-gyres, (i.e. ψ >25.9 Sv; the stippled area in Fig. 2d).

4.1   Part one: the large-scale investigation of heat within the Weddell Gyre

The heat budget contributions from the different terms in Eq. 1.2 (including the signs of each term, e.g.,$-\nabla_H U\theta$ and $+\kappa_H \nabla^2 \theta$) are provided in Fig. 2. While for the gyre at large, the mean horizontal geostrophic heat advection (Fig. 2a) shows a patchwork

210   display of heat transport convergence (positive) and divergence (negative), the southern limb of the gyre is generally dominated by heat transport convergence, of about +20 W m⁻² west of the Prime Meridian. A small patch of divergence is found over the western sub-gyre of about -10 to -20 Wm⁻² (~35-45°W, ~65°S), and over Maud Rise of about -20 to -30 Wm⁻² (~3°W, 65°S). The whole region east of the Prime Meridian is dominated by particularly strong patches of positive and negative values in excess of ±80 W m⁻². Along the northern limb of the gyre, the pattern is dominated by bands of alternating positive and negative

215   values, of about ±60-80 W m⁻², which are aligned in a manner that appears to follow the complex bathymetry in the region.

The heat flux due to mean vertical advection (-$w_E(\Theta_{mT} - \Theta_{mT-1000})$, Fig. 2b) is positive throughout, and considerably weaker than that due to mean horizontal advection, in the range of ~0-3 W m⁻². Vertical advection is weakest west of ~10°W, and strongest over the eastern sub-gyre region between 0 and 30° E. That the entire region shows positive vertical fluxes (with the exception of north of the Weddell Gyre) results from two factors: (1) the mean Ekman pumping velocity is positive (indicating

220   upwelling) throughout the offshore Weddell Gyre (downwelling, i.e. negative Ekman pumping velocity, is found in regions shallower than 2000 m and thus outside of our region of Argo float data availability) (Fig. S3), and (2) the upper boundary displays lower temperatures than the lower boundary (Fig. S1a), which is a consequence of the vertical boundaries applied in this analysis. Positive vertical advection implies that more heat is advected upwards into the core layer of WDW from below than is leaving by advection through the top, implying a convergence of heat within that layer, unless it is removed through

225   other mechanisms such as mean horizontal advection or turbulent diffusion.

Horizontal turbulent diffusion (Fig. 2c) is characterised by a positive signal of about 0-40 Wm⁻² within the IC, and a negative signal along the SL in the range of 20-60 Wm⁻², with the exception of local patches of heat flux convergence such as over Maud Rise and just north of Astrid Ridge at ~10°E (topographic features are marked in Fig. 1). The northern limb of the Weddell Gyre is mostly positive, (40-100 Wm⁻²), though a strip of heat flux divergence sits directly north of this area of heat

230   flux convergence, in the northern boundary zone between the Weddell Gyre and the Antarctic Circumpolar Current.

As with mean vertical advection, vertical turbulent diffusion (Fig. 2d) exhibits a uniform sign throughout the Weddell Gyre, with negative values in the range of -2 to -7 Wm⁻². The strongest values are found in the southern limb, at about ~20°E (~ -7 Wm⁻²), as well as just west of Maud Rise. There also appears to be slightly enhanced vertical turbulent diffusion along the gyre axis between about 10°E and 20°W.

235   The heat tendency resulting from the sum of the heat budget terms (left-hand side of eq. 1.2). is provided in Fig. 2e. There is
       a patchwork of negative (cooling) and positive (warming) values throughout, and overall Fig. 2e is spatially mostly similar to
       the heat flux due to mean horizontal advection in Fig. 2a. There is, however, a discernible cooling throughout the open southern
       limb in Fig. 2e, in comparison to Fig. 2a, and a clear warming along the northern limb, driven by horizontal turbulent diffusion
       (Fig. 2c). Any non-zero value in Fig. 2e should correspond to an area of warming (positive tendency) or cooling (negative
240   tendency) of the water column. Given that data from a 15 years-long observation period have entered the calculation, we
       wouldn't expect the real ocean to have experienced such a patchy warming and cooling pattern, resulting – in particular – from
       the horizontal advection field. In chapter 4.2 we therefore perform spatial integration of the fields displayed in Fig. 2a-e over
       distinct areas defined by the circulation (SL and IC), in order to eliminate some of the noise, such that more robust statements
       on the main balances between the different heat flux terms can be made on a regional scale. The uncertainties will be discussed
245   further in chapter 5.

(2a)

(2b)

(2c)

(2d)
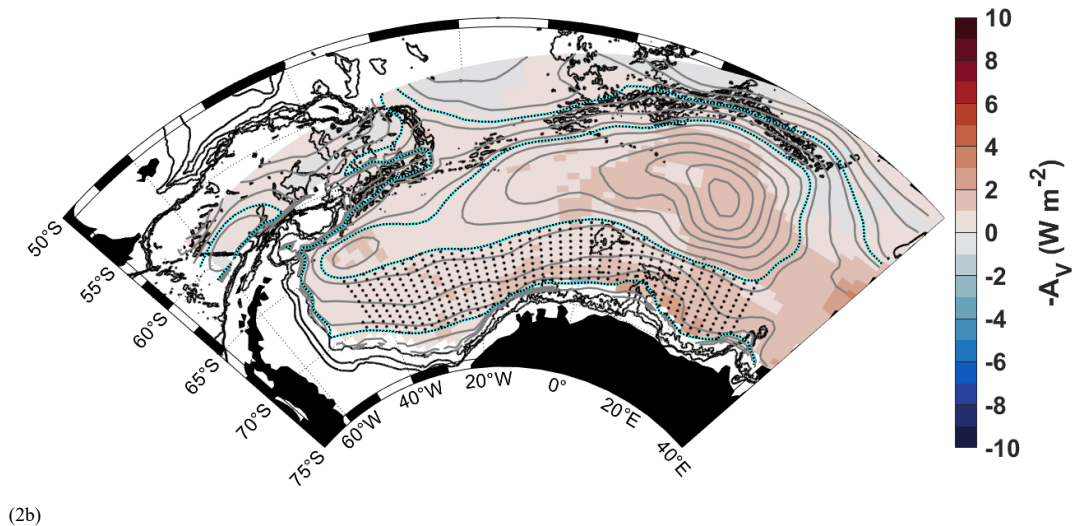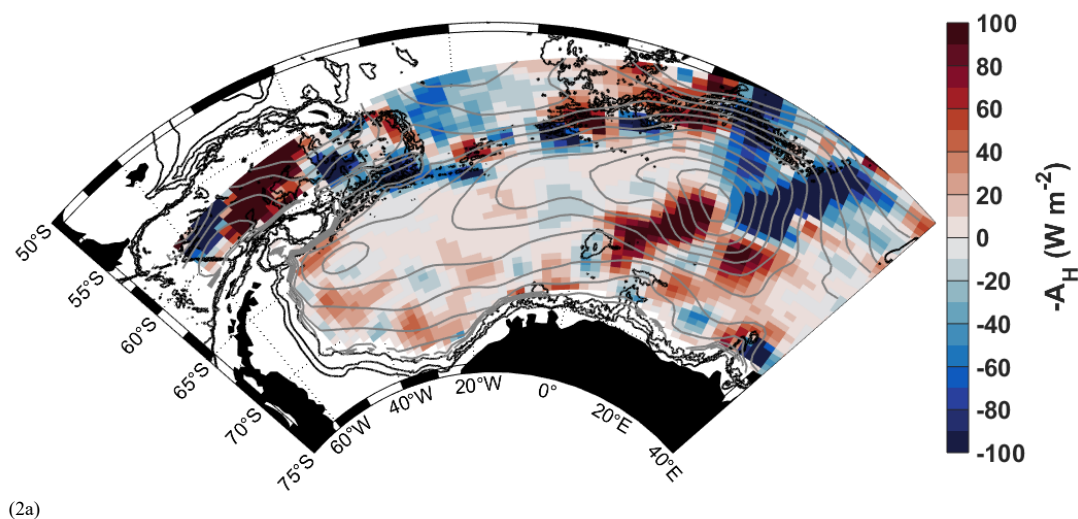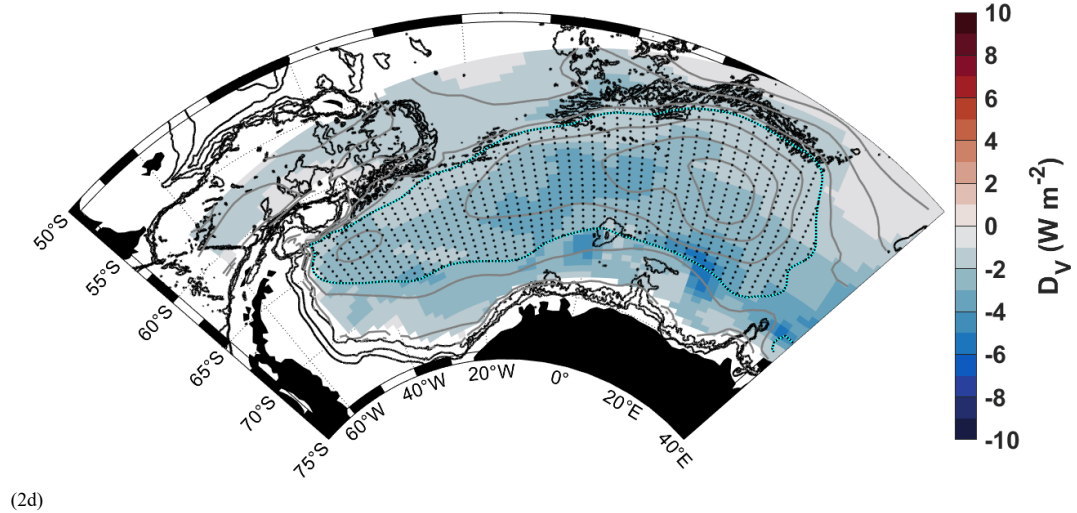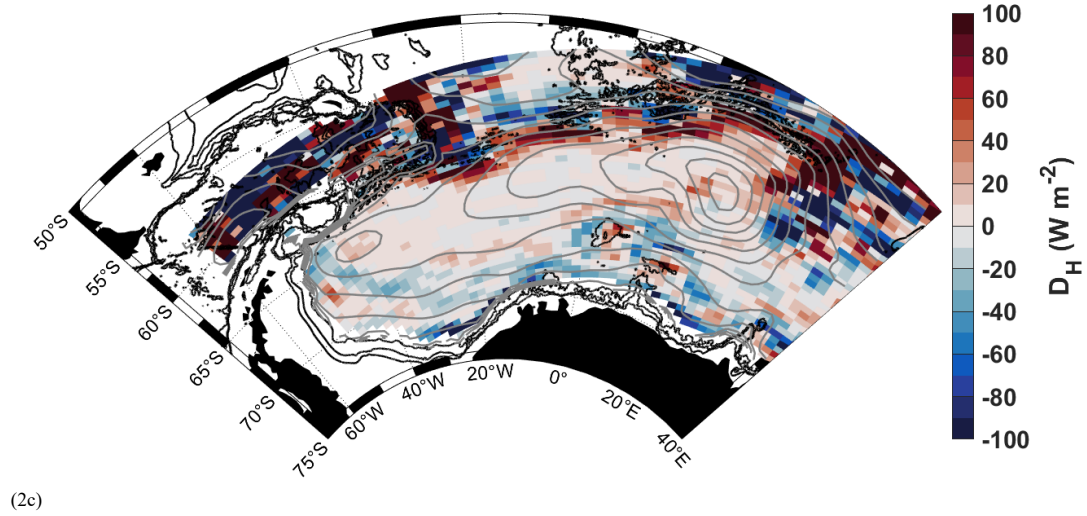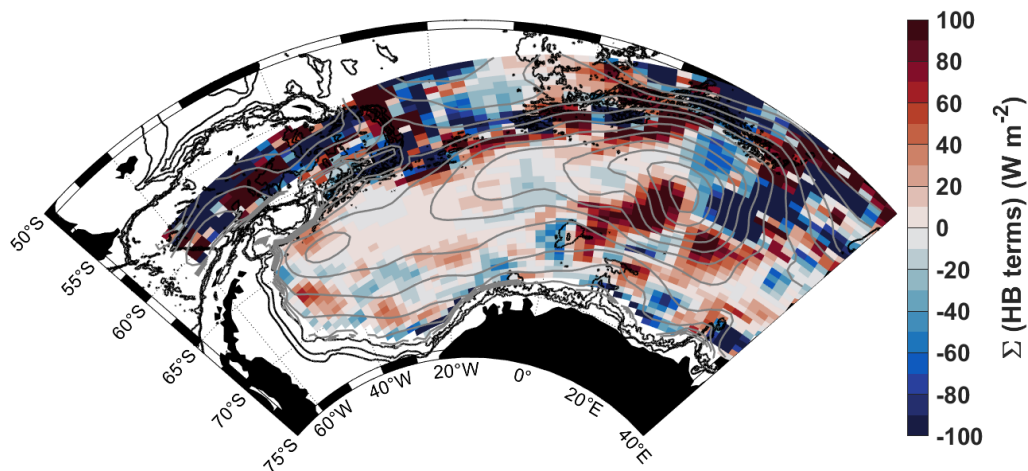
(2e)

Figure 2: The heat budget terms from Eq. 1.2, for a layer of water 1000 m thick from the depth of the mid-thermocline: (a) mean horizontal geostrophic heat advection, (b) mean vertical advection, (c) horizontal turbulent diffusion (d) vertical turbulent diffusion and (e) the sum of the terms in a-d. Positive values indicate warming, i.e. heat transport convergence, where more heat is entering the grid cell than is leaving it, whereas negative (blue) values indicate cooling, i.e. heat transport divergence, where more heat is leaving the grid cell than is entering it. Grey and black contours provide the horizontal streamlines and the 1000, 2000 and 3000 m isobaths respectively (as in Fig. 1). The stippled areas in Figs. b and d show the regions defined as SL and IC respectively, encased in the blue streamlines used to define the SL and IC regions. These regions are horizontally integrated across in the following Section 4.2. Note the different colour scales for the horizontal versus vertical fluxes.

4.2   Results part 2: zonal variation in the heat budget

In this section, we provide an analysis of the zonal variation of the heat budget in the Weddell Gyre of the two regions described at the beginning of Section 4 (highlighted in Figs. 2b and d). This is carried out as follows: we integrate meridionally for each zonal band in our data grids, from just west of Gunnerus Ridge (~33° E) in the westward direction towards the Antarctic Peninsula (Figs. 3-4, upper panel). The latitudinal range of the band is defined using the stream function, focusing on the SL and the IC. Lastly, we plot the cumulative zonal integration from east to west (Figs. 3-4, lower panel) and provide the zonally integrated heat budget terms in Table 3. We also take the sum of the heat budget terms and divide by the time period to get the temperature change for SL and IC, also listed in Table 3. For both regions, the zonal variation in the heat budget terms (Fig. 3-4, upper panel) show large local imbalances in the overall heat budget, which are physically implausible. However, useful information is provided in the net (zonally integrated) heat budget terms (Fig. 3-4, lower panel). The resulting volume integration describes the heat flux divergence (negative) or convergence (positive), owing to heat fluxes across the boundaries of the volume of water in question. By considering the 4 different heat budget terms with respect to each other, we can build up a picture of how and where heat is redistributed throughout the Weddell Gyre. Table 2 provides a list of the abbreviations for the terms presented in Figs. 3-8. The method for computing the associated errors is detailed in Section 3.2 as well as the Supplement (S7).

Region 1: SL (southern limb)

The SL region (Fig. 2b) spans the entire zonal extent of the double gyre system, with the northern boundary being the largest streamline that spans both sub-gyres, from just west of Gunnerus Ridge to ~45° W (30 Sv), and the southern boundary being the southernmost streamline that does not break into the coastline (16 Sv). This enables us to focus on the water that circulates the entire zonal extent of the gyre, thus reaching into the south-western interior.

Overall, the primary sources of heat (heat flux convergence) are from the advection terms, mean horizontal advection (A_H) and mean vertical advection (A_V), whereas the primary heat sinks (heat flux divergence) are from the turbulent diffusion terms, horizontal turbulent diffusion (D_H) and vertical turbulent diffusion (D_V) (Fig. 3, lower panel). The vertical terms are spatially invariant and contribute to the heat budget to a much lesser extent than the horizontal terms. This compliments the findings in

270 Fig. S2 of the net air-sea heat fluxes, which shows a relatively small heat loss through the surface of the ocean in the SL region. The heat flux convergence due to vertical advection is driven by upwelling, which leads to an advection of warm water upwards into the layer, whereas heat flux divergence due to vertical turbulent diffusion removes heat from the layer through the upper boundary (the mid-thermocline). Thus, heat enters the SL primarily through horizontal advection, and to a lesser extent by vertical advection due to upwelling, and is removed from the layer primarily by horizontal turbulent diffusion and vertical

275 turbulent diffusion (a small amount of which may escape through the surface of the ocean). Thus, the turbulent diffusion terms redistribute the heat that is advected into the gyre.

The largest regional fluctuations (Fig. 3, upper panel) in the sum of the terms are caused by large fluctuations in mean horizontal advection, in particular upstream of Maud Rise (i.e., mean horizontal advection increases by ~55 Wm^{-2} just east of the Maud Rise seamount, from 10° to 7° E, and then sharply decreases by ~80 Wm^{-2} from 7° E to the Prime Meridian). The

280 effect of Maud Rise is also visible in the net contribution (lower panel of Fig. 3), where it results in an increase in mean horizontal advection of ~7 TW from ~10° to ~5° E, after which a small decrease of ~2 TW occurs from 5° E to the Prime Meridian. This influences the net heat tendency (sum of the heat budget terms), which increases from 0 to ~7 TW, and then decreases to ~4 TW over the same longitudinal range. The perturbation in mean horizontal advection at Maud Rise is an artefact of being unable to resolve the regional circulation around Maud Rise, whereas the gridded temperature captures the

285 presence of the relatively cold Taylor Column situated over Maud Rise (clearly visible in Fig. 1). This creates strong horizontal temperature gradients on the eastern and western flanks of Maud Rise, i.e., in the direction of the dominant flow. This is discussed further in Section 5.2.2.

Region 2: IC (Interior Circulation cell)

The IC region (Fig. 2d) spans the entire zonal extent of the double gyre system, this time forming a fully enclosed circuit to

290 focus on the recirculating waters of the gyre, from just west of Gunnerus Ridge to near the continental shelf edge of the northern tip of the Antarctic Peninsula (~50° W).

Overall, the magnitudes of the heat budget terms are similar in the IC to the SL, with the exception of the mean horizontal advection term, which has a larger magnitude in the SL (10±15 Wm^{-2}) than in the IC (-2±24 Wm^{-2}) (Table 3). Note the differences in the magnitudes of the net heat budget terms are due to the larger area of the IC (Table 3). As with the SL, vertical

295 terms in the IC remain zonally spatially uniform and are much smaller in total magnitude than the horizontal terms, with heat being vertically advected into the IC domain (via upwelling) and removed from the IC domain by vertical turbulent diffusion. In contrast, the horizontal terms in IC change sign in comparison to the SL. Horizontal turbulent diffusion (D_H) is the primary heat source (i.e., heat flux convergence), whereas horizontal mean advection (A_H) is the primary heat sink (i.e., heat flux divergence) (Fig. 4, lower panel). Additionally, in contrast to the SL, the surface heat fluxes in this region (Fig. S2) are positive,

300 implying a positive heat flux into the ocean through the surface. This heat does not appear to cross the thermocline (i.e., the upper boundary of our domain), given the convergence of heat due to vertical advection and the positive vertical velocity values in Fig. S3 imply that, in the vertical, heat is entering the IC domain from below (due to upwelling), and vertical turbulent diffusion provides a heat sink (removal of heat), likely upwards through the thermocline, owing to the strong vertical temperature gradients associated with the thermocline. Thus, the heat entering through the ocean surface is likely to be

305 redistributed by other processes (such as surface transports or ice melt).

The largest regional fluctuations within the IC (Fig. 4, upper panel) in the sum of the terms are caused by two large peaks in mean horizontal advection, east of Maud Rise, where mean horizontal advection fluctuates from -65 Wm^{-2} to 50 Wm^{-2} and then to 6 Wm^{-2} over ~1400 km (from 28 to 12 to 7 °E). We assume these peaks are somewhat an artifact of the mean circulation interacting with strong lateral temperature gradients in the eastern sub-gyre region (i.e., the red and blue ellipses in Fig. 2e

310   over the eastern-sub-gyre coincide with strong temperature gradients in Fig. 1 and S5b), which is further discussed in Section 5.2.2.

Table 2: Explanations of the abbreviations used in Figs. 3-8.

Term	Description
A_H	Mean horizontal geostrophic heat advection
A_V	Mean vertical heat advection
D_H	Horizontal turbulent diffusion
D_V	Vertical turbulent diffusion
$\overline{\sum AD}$	The sum of the heat budget terms in Eq. 1, listed above, where A stands for the horizontal and vertical advection terms and D stands for the horizontal and vertical diffusion terms.
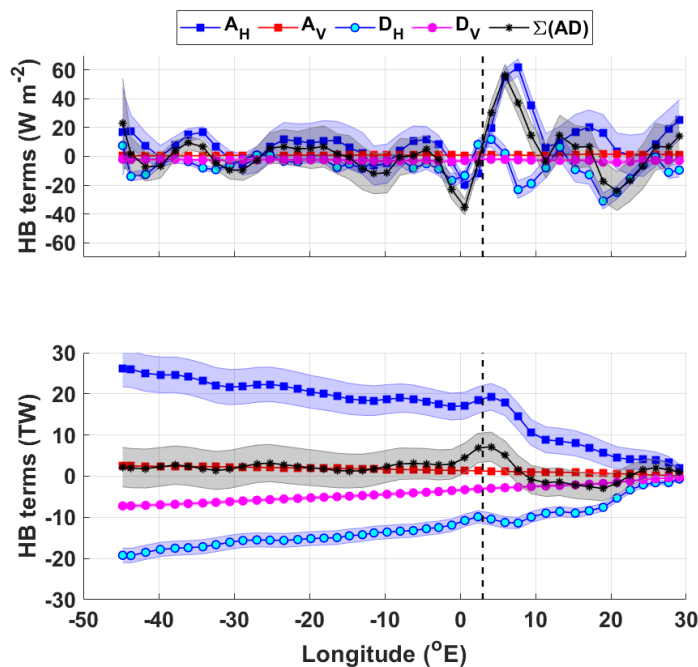
Figure 3: upper panel: the heat budget terms for the southern limb (SL) of the gyre in Wm^{-2}; lower panel: the cumulative heat budget terms in Terawatts (TW). The key for the legend is listed in Table 2. The dashed vertical line marks the approximate longitude of Maud Rise, at 3° E.
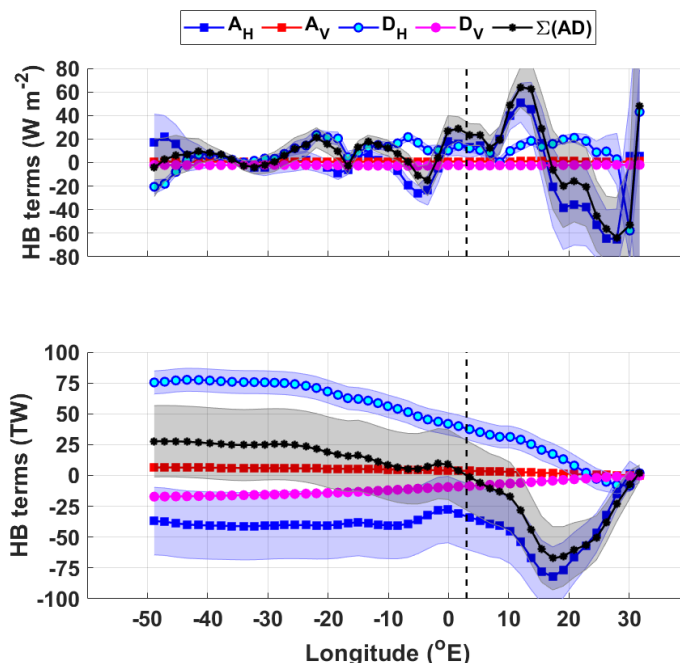
Figure 4: As in Fig. 3, but for the interior circulation cell (IC) of the Weddell Gyre.

Table 3: Zonal mean (W m^{-2}) and net (TW) heat budget contribution of the different terms in Eq. 1.2 for the SL and IC zones of the Weddell Gyre (Fig. 3 and 4 respectively), and an estimate of temperature change (dT/dt), using a time period of 14 years. The uncertainty provided for the net heat budget terms (in TW) are the sum in quadrature of the propagated errors. For the mean heat budget terms (in W m^{-2}), the provided uncertainty is the standard deviation of the zonal mean heat budget term, and the mean error (in Wm^{-2}) is the mean of the propagated error and the standard deviation of the mean propagated error. See Section 5.2 for further information.

Heat Budget Term	SL			IC		
	Mean (W m^{-2})	Mean Error (W m^{-2})	Net (TW)	Mean (W m^{-2})	Mean Error (W m^{-2})	Net (TW)
Mean Air-Sea flux	-1.8		-4.6	+8		+60
Mean horizontal advection	+10 ± 15	10 ± 5	+26 ± 4	-2 ± 24	17 ± 22	-37 ± 27
Mean vertical advection	+0.9 ± 0.3	0.1 ± 0.04	+2.5 ± 0.03	+0.8 ± 0.2	0.05 ± 0.04	+6.5 ± 0.1
Horizontal turbulent diffusion	-6.7 ± 8.6	4 ± 2	-19.0 ± 2	+8.7 ± 14	5 ± 6	+75 ± 9
Vertical turbulent diffusion	-2.7 ± 0.5	0.9 ± 0.2	-7.2 ± 0.4	-2.3 ± 0.3	0.6 ± 0.1	-17 ± 0.6
Heat tendency (i.e., sum of the heat budget terms)	+1.6 ± 16	11 ± 5	+2.2 ± 5	+5.5 ± 26	17 ± 22	+28 ± 29
Temperature tendency over 14 years (°C)			+ 0.09 ± 0.2 °C or +0.006 ± 0.01 °C/yr			+ 0.4 ± 0.4 °C or 0.03 ± 0.03 °C/yr

315

In order to learn more about how the heat budget terms act to redistribute heat throughout the IC, we further split the IC into

IC-north (Fig. 5) and IC-south (Fig. 7), where the interface between the two regions is defined as the central gyre axis (i.e., the

zonal maximum stream function, north of which the flow is predominantly eastward, south of which the flow is predominantly westward). When integrating over these smaller regions, the heat budget does not close. We can, however, learn more about

320   the processes which provide heat sources and sinks to these different regions. The first challenge that emerges is the non-objective decision-making required regarding whether to include the easternmost part of the IC, where the horizontal mean advection may be unrealistic. We remove the eastern most values, east of 25°E in the IC-north, and focus only on west of Maud Rise (inclusive of Maud Rise) for the IC-south. We choose these limits in order to remove the anomalous ellipses that extend diagonally north-eastwards from Maud Rise. To further investigate horizontal diffusion, we computed horizontal

325   turbulent diffusion heat fluxes across three zonal boundaries: (1) across the northern boundary of the gyre (defined as the northernmost streamline of the filled region in Fig. 2d i.e., the streamline that, in Fig. 2c, marks the boundary between heat flux convergence within the Weddell Gyre (red) and heat flux divergence to the north (blue)); (2) across the interface between the divergence zone within the SL and the convergence zone in the IC; and (3) across the central gyre axis from IC-south into IC-north, for west of Maud Rise. The zonal variation in heat flux for each boundary is provided in Fig. 5b and 7b-c respectively,

330   whereas the zonal integrations of the fluxes are provided in the Supplements (Fig. S6).

Horizontal turbulent diffusion is the dominating heat source to the IC-north, providing a net 78 ± 4 TW of heat, whereas horizontal mean advection is a net heat sink, removing 68 ± 15 TW (Fig. 5a). Half the horizontal turbulent diffusive flux of heat occurs along the northern boundary of the gyre (32 ± 1 TW), with particularly large southward heat fluxes (>200 Wm^{-2}) directly downstream of the South Sandwich Trench, and in the region of the southwest Indian Ridge east of 10°E (Fig. 5b),

335   indicating that the rest of this heat flux occurs in the easternmost part of the IC-north. The large fluxes are most likely due to the strong meridional temperature gradients characteristic of the boundary between the warmer ACC to the north and the colder Weddell Gyre to the south.

Overall, when looking at the zonal variation in the heat budget terms in Fig 5a (upper panel), the positive peaks in horizonal turbulent diffusion are synchronous with the troughs in horizontal mean advection, implying that as heat is turbulently diffused

340   across the boundary into the IC-north, horizontal advection "carries" this heat away along the eastward-flowing northern limb of the gyre. We can also demonstrate this by following the evolution of the sub-surface temperature maximum along a single streamline (in this case, Ψ=26 Sv, which is the outer boundary of the IC, as shown in Fig. 2d), which shows an overall increase in temperature along the northern limb of the Weddell Gyre, as well as an overall decrease in temperature along the southern limb of the Weddell Gyre (Fig. 6).
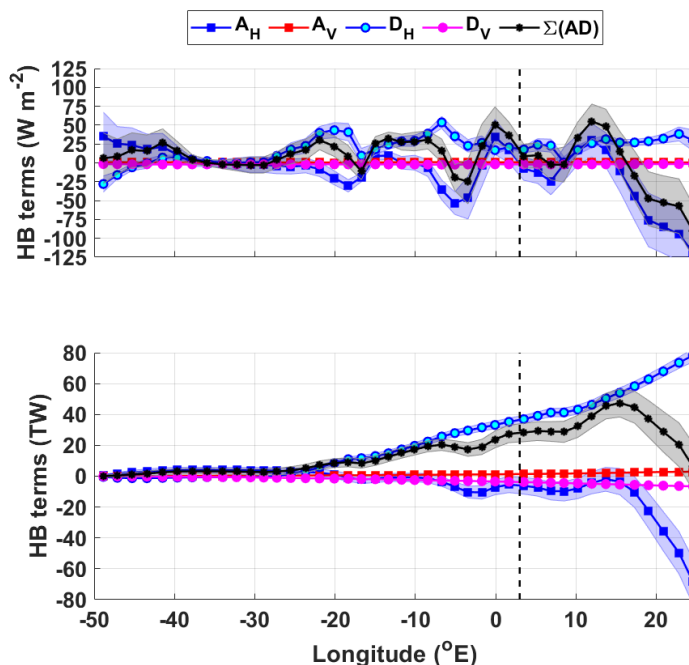
(a)
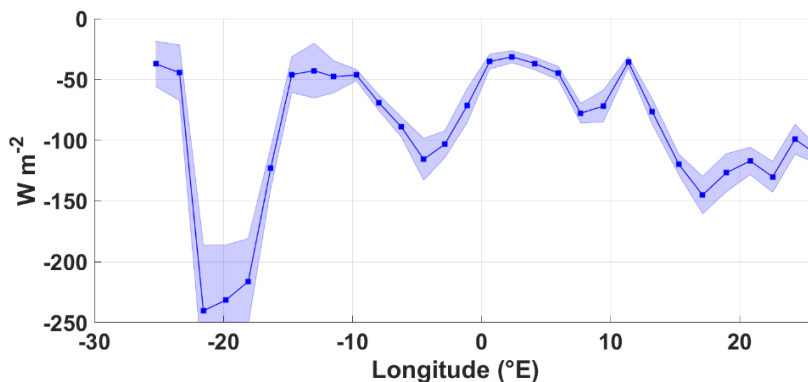
(b)

Figure 5: (a) Heat budget terms for the IC-north, west of 25°E: upper panel: zonal means in Wm^{-2}; lower panel: the cumulative heat budget terms from west to east in Terawatts (TW). The key for the legend is listed in Table 2. The dashed vertical line marks the approximate longitude of Maud Rise, at 3° E. Panel b shows the zonal variation of the diffusive horizonal heat flux across the northern boundary of the northern limb of the Weddell Gyre, in W m^{-2}, defined by the streamline that equals 25 Sv. Negative values indicate a southward flux of heat into the eastward-flowing northern limb of the Weddell Gyre from north of the northern Weddell Gyre boundary (the subsequent cumulative horizontal diffusive heat flux across the northern boundary is provided in the Supplements in Fig. S6a).
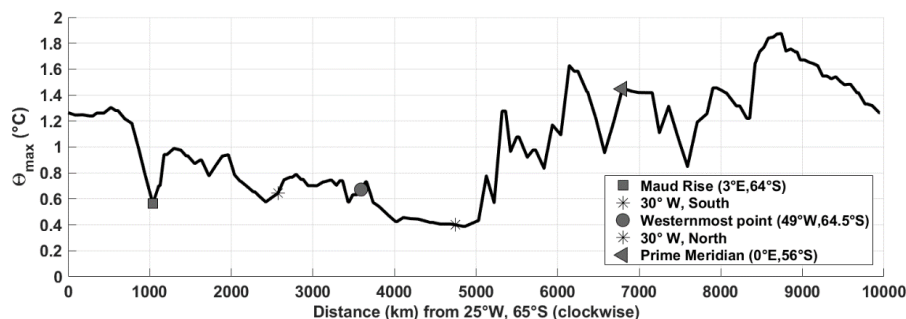
Figure 6: θ_{max} (°C) along the streamline Ψ = 26 Sv (i.e., the outermost boundary of the IC). The distance in km is along the streamline in a clockwise direction from 25°W, 65°S, with key locations marked using the legend.

345

Horizontal mean advection provides a heat sink of 3 ± 3 TW in the IC-South directly west of the Prime Meridian, up until ~10°W (Fig. 7a), after which it provides an overall heat source (7 ± 3 TW). The initial heat sink could be indicative of heat advection following the mean circulation about the eastern sub-gyre, as indicated by the streamlines in Fig. 2; west of this, heat is advected into the area that circulates the western sub-gyre. In contrast to the SL, horizontal turbulent diffusion is also a

350   source of heat to this area (3.3 ± 1 TW), which is indicative of a northward diffusive heat flux, which removes heat from the SL, transporting it northwards into the IC-south. This is indeed the case when computing the diffusive heat flux across the northern boundary of the SL in Fig. 7b, which gives a net heat flux of 6.4 ± 0.6 TW, of which 3.4 ± 0.6 TW occurs downstream of Maud Rise (Fig. S6b). Additionally, a net diffusive heat flux of 0.8 ± 0.1 TW occurs northwards from the IC-south across the central gyre axis into the IC-north, mainly occurring 10-28°W, i.e., at the interface between the eastern and western sub-

355   gyres (Fig. 7c & S6c). The diffusive flux of heat northwards from the SL into the IC occurs at a mean rate of 22 ± 12 W m^{-2} (Fig. 7b), with a maximum at 10° E, of ~50 ± 25 W m^{-2}, where the streamline along which we are integrating starts to curve northwards to meander around the northern flank of Maud Rise. The streamlines indicate a strong flow in this region, with a sharp meridional gradient between the colder recirculated water close to the central gyre axis, and the relatively warm advected inflow of the southern limb. The main heat sink in the IC-south is the vertical turbulent diffusion term (Fig. 7a), which removes

360   6 ± 0.3 TW upwards through the thermocline.
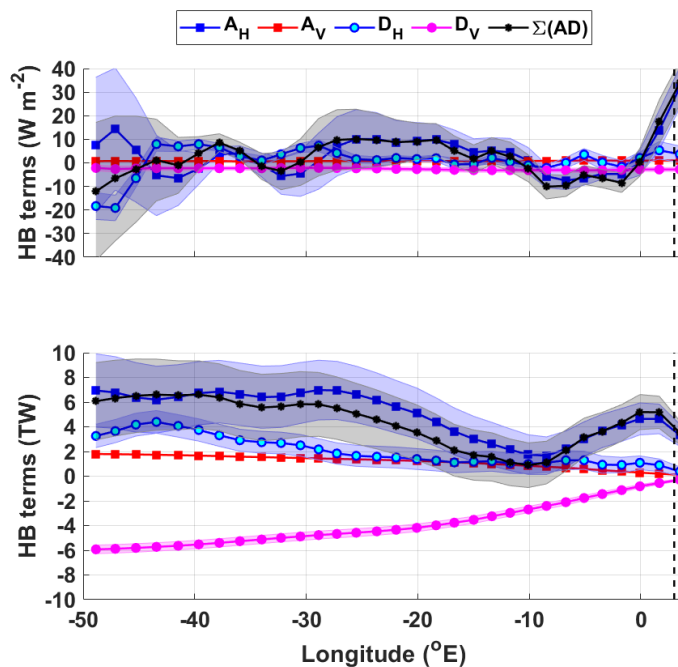
(a)
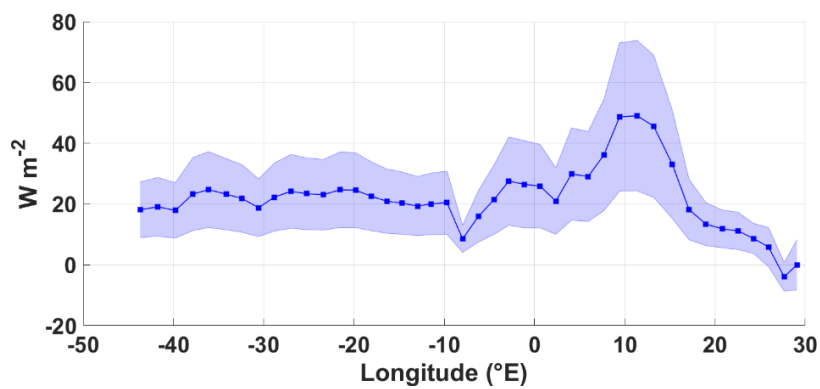
(b)
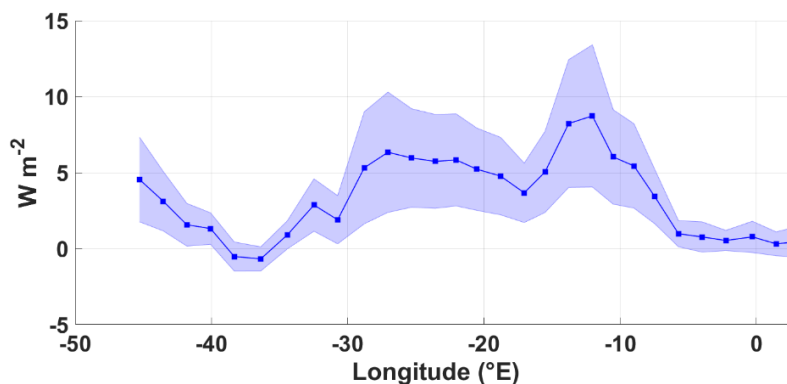
(c)

Figure 7: (a) Heat budget terms for the IC-south, west from ~3°E (Maud Rise): upper panel: the heat budget terms in Wm⁻²; lower panel: the cumulative heat budget terms in Terawatts (TW). The key for the legend is listed in Table 2. The dashed vertical line marks the approximate longitude of Maud Rise, at 3° E. Panels b and c show the zonal variation of the diffusive horizontal heat flux in W m⁻² for (b) across the boundary between the SL and the IC, and (c) across the central gyre axis from the IC-south to the IC-north, west of Maud Rise. Positive values indicate a northward flux of heat from the SL into the IC, and from the IC-south northwards into the IC-north, respectively (the subsequent cumulative horizontal diffusive heat flux across the northern boundary is provided in the Supplements in Fig. S6b-c).

5   Discussion

In this study, velocity and temperature derived from Argo floats were used to determine the heat budget of the Weddell Gyre,

365   for a 1000 m thick layer of water extending from the mid-point of the thermocline, encompassing the core of the WDW layer. In the following section, we provide an in-depth discussion of the study limitations, before ultimately discussing and interpreting the results in Section 5.2.

5.1   Study limitations

Before interpreting the results, several limitations of the study require discussion.

370   #### 5.1.1   Vertical boundary limits

The first limitation relates to the omission of the upper 50 dbar from the profiles prior to mapping (Supplements S1), to avoid the highly seasonally varying surface waters. Ideally, we would include the upper ocean layer, in order to explicitly apply the net air-sea heat flux term (Qnet) as a surface boundary condition in the heat budget equation. Since we are interested in the re-distribution of heat throughout the Weddell Gyre (with the main heat source being the WDW), we applied boundary conditions

375   which ensure that the Winter Water layer (defined by its temperature-salinity minimum) is not included within the subsurface layer of interest, while the core of WDW (i.e., Θ_{max}) is fully included. The vertical boundary conditions allow us to consider the varying depths of the upper boundary, while also avoiding bias by fixing the thickness of the vertical layer. However, this may introduce some noise into the analysis from grid cell to grid cell, owing to the different depths of the water column the heat budget is integrated over. This may partly explain why there is considerable noise in the maps in Section 4.1, while the

380   noise partially cancels out in Figs. 3 and 4. The implication is that our heat budget analysis is reasonable on large-scales, but would introduce considerable noise when assessed on local-scales. We return to this when discussing regional imbalances in Section 5.2.2, and find that the lateral gradients in the upper boundary depth are unlikely to be a major source of the noise in Fig. 2 (Fig. S5a).

5.1.2 Estimating vertical velocity

385   Another limitation in the study is a suitable estimate for vertical velocity. Vertical Ekman pumping velocity is used to represent
vertical velocity, which is held constant with depth (Supplements S3) throughout the 1000 m thick layer, thus assuming a
perfect geostrophic (thus non-divergent) flow. However, reanalysis-based wind products from which w_E is computed, are also
limited in their accuracy, largely due to lack of in-situ wind measurements in the Southern Ocean. Additionally, vertical
velocities resulting from eddies, fronts and along steeply sloping bathymetry are not taken into account in this study, which
390   might be important sources of vertically non-uniform vertical velocities in the upper ocean.

5.1.3 Diffusivity

The work presented within this paper is based on a long-term mean gridded dataset derived from Argo floats between 2002
and 2016 (Section 2.2). Thus, we are unable to directly incorporate an eddy component into the analysis, which requires
fluctuations from the mean temperature and velocity (i.e., u'T'). Unresolved eddying fluctuations are most likely to be an
395   important factor when assessing the heat budget east of the Prime Meridian in the Weddell Gyre, a region we know to be
dominated by a mesoscale eddy field (e.g., Schröder & Fahrbach, 1999; Leach et al., 2011; Ryan et al., 2016). Meanwhile,
within this study, we rely on the parameterization of eddy-influences through the estimation of horizontal turbulent diffusion,
and the parameterization of vertical instabilities through the estimation of vertical turbulent diffusion. Horizontal and vertical
diffusivity (κ_H and κ_v in Eq. 1) yield considerable uncertainty to this study, especially where they are assumed constant in
400   space. Horizontal diffusivities have been shown to be length scale-dependent (Okubo, 1971; Ledwell et al., 1998). For
example, Ledwell et al (1998) demonstrate the importance of length scales in the Eastern North Atlantic by releasing and
following the dispersal of a patch of sulphur hexafluoride, estimating values of 2 m^2 s^{-1} for length scales of 1-10 km, and as
much as 1000 m^2 s^{-1} for length scales of 30-300 km. For the entire Southern Ocean, Zika et al. (2009) estimate a value of 300
± 150 m^2 s^{-1}. Within the Weddell Gyre, Leach et al. (2011) provide estimates of κ_H and κ_v derived from observations in the
405   Maud Rise region, and estimate κ_H to be in the range of 70-140 m^2 s^{-1}. Leach et al. (2011) consider their estimate for κ_H
appropriate, albeit on the low side, for mesoscale eddies (although the station spacing of the observations in their analysis is
55 km; not the ~10 km corresponding to the baroclinic Rossby radius in the region). For the Weddell Gyre, Donnelly et al.
(2017) provide estimates of κ_H derived from observations (WOCE CTD stations from 37 hydrographic sections) on a larger
scale than that of individual eddies, where κ_H is estimated as 247 ± 63 m^2 s^{-1}. Cole et al. (2015) use salinity anomalies from
410   Argo floats and velocity fluctuations from the ECCO2 product, which is an ocean state estimate that assimilates data
(Menemenlis et al., 2005, 2008) to investigate horizontal mixing and the associated length scales. In Fig. 4 of Cole et al. (2015),
at about 50 to 60° S in the Atlantic Ocean (the most southerly extent of the authors' analysis), the estimated values of κ_H range
from 200 to 2000 m^2 s^{-1} in the depth range of 0 to 2000 m. In Sevellec et al., (2022), the authors provide a useful dataset of κ_H
at 1000 m, derived using Argo float trajectories: this is only possibly when a sequence of positions are available, from which
415   the authors derived a "pseudo-trajectory". Thus, most of the Weddell Gyre resembles a data gap, with the exception of the
Prime Meridian and the north and eastern peripheries of the gyre. These values vary between 0 and 8000 m^{2}s^{-1}; and are close
to zero around Maud Rise, and can be 4000-8000 m^{2}s^{-1} within the eastern and northern gyre periphery. In this study, we are
focused on the large-scale, and have a grid of data representative of the long-term mean from 2002-2016. Our grid cell
resolution varies slightly with changing latitude (Reeve et al., 2019), but is on the order of ~80 x 60 km, which is nearly double
420   the station spacing of 55 km in Leach et al. (2011). The length-scales applied in the objective mapping are 800 km in stage 1
and 400 km in stage 2, with a skew on the shape of the radius of influence based on the range in potential vorticity (See Section
2.2 in Reeve et al., 2019), and therefore the length scales upon which the analysis falls would actually be considerably greater
than in Leach et al. (2011), but with similarities to the length-scale assumed in Cole et al. (2015) of 300 km. We make the
decision to use the Sevellec et al. (2022) dataset where numerous data are available, and, for within the Weddell Gyre, we
425   arbitrarily provide a baseline range of potential values for horizontal diffusivity, in the range of that provided by Donnelly et
al. (2017), Zika et al. (2009) and more specifically Cole et al. (2015), of 400 ± 200 m^2 s^{-1} (the ranges are incorporated into the

error propagation computation). A detailed explanation of our method and reasoning regarding the Sevellec et al (2022) dataset is provided in the Supplements (S4).

Referring now to the vertical diffusivities, Leach et al. (2011) provide particularly small estimates for κ_v, of 3 x 10^{-6} m^2 s^{-1} for
430 the core of WDW, which they suggest is due to the timing of the survey – having taken place late spring/early summer, when sea-ice had just melted, and the wind had not yet had time to stir up the water column. Other studies provide larger estimates for κ_v, for various regions throughout the global ocean. Donnelly et al. (2017) estimate κ_v as 2.4 ± 2.8 x 10^{-5} m^2 s^{-1}. Over rough topography, such as 500 m above abyssal sea mounts on the flanks of the mid-Atlantic Ridge in the Brazil basin, Ledwell et al. (2000) provide an estimate for κ_v of 3 x 10^{-4} m^2 s^{-1}. Over flat bathymetry of the ocean's abyss, however, Polzin et al. (1997)
435 and Ledwell et al. (1998) estimate κ_v to be about 1 x 10^{-5} m^2 s^{-1}. Naveira Garabato et al. (2004a, 2004b, 2007) provide larger numbers for deep water in the Scotia Seas of 3 x 10^{-4} to 1 x 10^{-2} m^2 s^{-1}, which they attribute to breaking internal waves. Also within the Southern Ocean, Cisewski et al. (2005, 2008) acquired 7 x 10^{-4} m^2 s^{-1} in the upper pycnocline of the Antarctic Circumpolar Current at 20° E and Forryan et al. (2013) obtained a value of 1.9 x 10^{-5} m^2 s^{-1} based on observations in close proximity to a vigorous frontal system between 60 and 80° E, at the northern edge of the Kerguelen Plateau.

440 Initially, we attempted to estimate κ_v through the use of the Richardson Number, following Forryan et al. (2013), defined as the ratio of buoyancy frequency (N) squared to vertical shear squared, and often used to describe the stability of stratified shear flow. For large Richardson Numbers, the resulting diffusivity tends towards a background diffusivity coefficient provided by the authors. In the Weddell Gyre, the circulation is mostly barotropic, and so the vertical shear is small, leading to large Richardson Numbers, especially when one is focused on the long-term mean. Thus, with this method, the resulting diffusivity
445 tends back towards a background diffusivity parameter. Hence, based on the range of values available from the literature, we made the decision to provide a range of potential values for vertical diffusivity, of (2.6 ± 2.4) x10^{-5} m^{2}s^{-1} (the "uncertainty" is incorporated into the error propagation computation).

A final consideration regarding uncertainty is related to using a simple differencing scheme at the grid cell resolution in order to compute spatial gradients in the heat budget equation (Eq. 1.2). Alternatively, we could have extracted curves from the grid
450 from which to determine the gradients. However, this is dependent on further length scales, which could introduce additional uncertainty, and may also result in additional smoothing of the observed fields. Thus, we applied the former method, which extracts the gradients directly from the gridded datasets at the grid cell resolution, with the expectation that this would result in large regional fluctuations owing to the coarse grid resolution.

455 ## 5.2 The Weddell Gyre heat budget

5.2.1 Overall findings

While the heat budget does not close on regional scales, it does approximately close when integrating over large areas, thus, important and useful information can be provided from comparing the four resulting heat budget terms.

In most regions of the Weddell Gyre, for the core of WDW, the terms dominating the heat budget are mean horizontal
460 geostrophic advection (Fig. 2a), and horizontal turbulent diffusion (Fig. 2c). Horizontal mean advection appears patchy, though generally implying warming (convergence) in the southern limb of the gyre (Fig. 2a). Horizontal turbulent diffusion (Fig. 2c) acts as a heat source (heat flux convergence) within the eastward flowing northern limb of the gyre and to a lesser extent the gyre interior. In contrast, horizontal turbulent diffusion is associated with a divergent heat flux (or loss of heat) in the open southern limb of the gyre, as well as directly north of the gyre. For the most part, mean vertical advection and vertical turbulent
465 diffusion are spatially relatively uniform, where upwelling advects heat upwards into the WDW layer, and vertical turbulent diffusion removes heat through the top of that layer, upwards through the thermocline to the overlying Winter Water (WW).

Additionally, the sum of the heat budget terms in Fig. 2e imply a general cooling in the SL, and a general warming in the IC, synchronous with the surface heat fluxes in Fig. S2, where the IC experiences a net heat flux into the ocean from the atmosphere, while in the SL the ocean loses heat to the atmosphere.

470   The spatial patterns in the heat budget terms become distinct when integrating over large areas, namely, the SL and IC (Section 4.2). While the vertical terms are spatially uniform throughout, providing a heat source (mean vertical advection) and a heat sink (vertical turbulent diffusion) throughout both regions, the horizontal terms "switch roles" in the SL versus the IC. Horizontal mean advection is a mechanism which brings heat into the SL, while horizontal turbulent diffusion removes much of that heat from the SL. In contrast, horizontal turbulent diffusion brings heat into the IC, whereas mean horizontal advection

475   provides a heat sink in the IC. Thus, while both mean horizontal and vertical advection are responsible for bringing heat into the core of the WDW layer of the Weddell Gyre, turbulent diffusion is the mechanism which then redistributes that heat throughout the gyre interior. Surface heat fluxes (Fig. S2) also imply that the upward diffusive heat flux through the top of the layer (i.e., the mid-thermocline) may represent a source of heat for the observed negative air-to-sea heat flux in the SL. In the IC, where air-to-sea heat fluxes are positive, the upward diffusive heat flux across the upper boundary of the WDW layer may

480   be horizontally redistributed by the upper ocean flow field and additionally may provide heat required to melt sea ice in this area.

5.2.2   Regional (im-)balances

When integrating over smaller regions, the heat budget does not close (see Figs. 2e, 3 and 4), indicating that noise is largely cancelled when integrating over larger areas. The noise is likely a result of (1) discrepancies in the depth range from grid cell

485   to grid cell, (2) the nature of differentiating across grid cells, (3) due the presence of mesoscale eddies unresolved by the data and methods used, and (4) aliased observations that result in a distortion of the mean state. Here, we discuss the influence of (1) unresolved mesoscale eddies and narrow currents in the eastern Weddell Gyre, (2) Maud Rise and (3) the open northern boundary, and discuss what might be missing that prevents the closure of our heat budget analysis.

The presence of unresolved mesoscale eddies is particularly important east of the Prime Meridian. In Fig. 1, it is clear there is

490   a misalignment between the streamlines and temperature distribution in the eastern part of the gyre; horizontal mean advection hugely dominates this region which is partially compensated by horizontal turbulent diffusion (Fig. 2). Given the domed shape of the isopycnals characteristic of a cyclonic gyre (e.g., Strass et al., 2020; Fahrbach et al., 2011), we hypothesised that a larger bias due to the horizontal gradient of the upper boundary depth (i.e., mid-thermocline, Fig. S1b) was occurring at the gyre periphery (i.e., where the slopes of the isopycnals are largest), which may be contributing to the large ellipses in horizontal

495   mean advection at the eastern periphery of the gyre in Fig. 2a. This appears not to be the case, given there is no clear large horizontal gradient in the mid-thermocline depth in the east; indeed, the largest horizontal gradient in mid-thermocline depth occurs in the very west of the Weddell Gyre, along the Antarctic Peninsula, and to a lesser extent over Astrid Ridge (Fig. S5a). The large ellipses do, however, appear to be related to large horizontal temperature gradients (Fig. S5b). We found the largest horizontal temperature gradients unsurprisingly along the northern boundary of the Weddell Gyre (owing to the considerably

500   warmer ACC to the north), but also in a diagonal line spanning from directly east of Maud Rise, northwards to the northeast of the eastern sub-gyre (~30°E, 55°S); in other words, synchronous with the north-easternmost ellipse of heat flux divergence and south-westernmost ellipse of heat flux convergence (Fig. 2a & 2e). The strong horizontal temperature gradients therefore likely accounts for the two strongest ellipses in Fig. 2. This, along with the fact that the computation (which relies on differencing across grid cells) is sensitive to the alignment of the temperature field to the velocity field, which is imperfect,

505   especially on such a coarse resolution grid. In particular, temperature is a more conservative (slow changing) variable in comparison to the velocity field. Thus, in capturing the mean state, our depiction of the mean velocity field may be especially distorted due to aliasing of observations, which we know are biased to summer conditions, and are particularly varying on shorter timescales in the dynamic region east of the Prime Meridian. In addition to the aliasing of the observations in

representing the mean state, it is possible that there is a significant additional component (in addition to mean horizontal
510   advection) which distributes heat in the eastern part of the gyre. The question is, how much of this is a result of unresolved
mesoscale activity driving large temperature and velocity gradients on much shorter length scales than can be appreciated here,
resulting in thus aliased observations, and whether the additional component is a real measurable yet unobserved (in this study)
component, or an artefact of the method and data sources used in this study. We know that the eastern part of the eastern sub-
gyre is dominated by an intense mesoscale eddy field (Ryan et al., 2016, Leach et al., 2011 and Gordon and Huber 1984),
515   where the boundary to the gyre is poorly-defined due to the openness of the topography. Indeed, Schröder and Fahrbach (1999)
suggest that there is no continuous current marking the eastern boundary, and that baroclinic shear instabilities lead to a
breakdown of the eastward-flowing current in the northern limb of the gyre, and that the current "reforms" in the westward-
flowing southern limb. This also aligns with the findings of Sonnewald et al. (In review), who use machine learning in a climate
model to diagnose the dominating dynamic regimes in the Southern Ocean, leading them to propose a circumpolar "super-
520   gyre" which connects the Weddell and Ross sub-gyre systems. In the far-eastern sub-gyre region, recirculated "cold-regime"
WDW (modified primarily through heat loss) comes into contact with incoming "warm-regime" WDW (Gordon and Huber,
1984). The "warm-regime" WDW represents relatively warm WDW advected into the gyre at the eastern inflow zone at about
30° E, driven by mesoscale eddies (Deacon 1979; Orsi et al. 1993; Orsi et al. 1995; Gouretski and Danilov 1993, 1994; Ryan
et al., 2016). It is therefore possible that horizontal turbulent diffusion, supposedly representative of turbulent dynamic
525   processes within this study, is underestimated in this region. This is also implied when comparing the two terms in Fig. 2a and
2c: while the magnitude is much larger in Fig. 2a (horizontal mean advection), horizontal turbulent diffusion displays the
opposite signs and partially compensates in the eastern sub-gyre region in Fig. 2c.

It could also be that there is a missing process, such as entrainment, that may account for the non-closure of the heat budget
terms in Fig. 2e (though entrainment would constitute a heat flux divergence which may help close the heat budget of the IC,
530   but not of the SL). Indeed, Schlosser et al. (1987) used Helium-3 tracers within the north-western Weddell Sea to estimate a
vertical diffusivity that is twice the value that we use here (5 x 10^{-5} m^2 s^{-1}) along with a rate of entrainment of WDW into the
overlying WW of 15-35 m yr^{-1}. Behrendt et al. (2011) argue that increasing WW salinity during 1992-1996 is caused primarily
by entrainment of WDW, and lists entrainment as one of three dominating causes of salinity changes to WW (the others being
sea-ice formation related salt release and horizontal advection). Brown et al. (2015) also highlight the important role of
535   entrainment in the carbon dynamics of the Weddell Gyre, by bringing dissolved inorganic carbon and salt upwards into the
WW from the underlying WDW. Given this work is based entirely on observations, and that we lack sufficient observations
to effectively resolve the complex dynamics of the eastern Weddell Gyre, the findings here illustrate the need for better
observational coverage of the Southern Ocean in the high latitudes east of the Prime Meridian, a region thus far often omitted
from observation campaigns.

540   Maud Rise is a prominent feature in temperature (Fig. 1), mean horizontal advection (Fig. 2a), horizontal turbulent diffusion
(Fig. 2c) and to a lesser extent, vertical diffusion (Fig. 2d). The effect of Maud Rise on WDW temperatures is due to the
presence of a Taylor column directly over Maud Rise, which has been previously observed as a stagnant column of relatively
cold water surrounded by a warm halo on the flanks of Maud Rise (e.g., Muench et al., 2001; Leach et al., 2011). Regarding
the heat budget terms shown in Fig. 3, mean horizontal advection results in a heat flux convergence upstream of Maud Rise,
545   which is partially balanced by heat flux divergence due to horizontal turbulent diffusion. In contrast, downstream of Maud
Rise, heat flux divergence occurs due to both mean horizontal advection and horizontal turbulent diffusion in Fig. 3 (although
a convergence peak in horizontal turbulent diffusion does occur directly over Maud Rise).

The effect of mean horizontal heat advection on the flanks of Maud Rise is probably mainly an artefact of the velocity field.
Since the water overlying Maud Rise is cold, and the velocity field does not adequately resolve the flow circulating the
550   seamount (instead the streamlines in Fig. 1 cut directly East-West across Maud Rise), the heat convergence upstream of Maud

Rise and divergence downstream of Maud Rise are caused by strong lateral temperature gradients between the cold water column overlying Maud Rise and the warm halo surrounding it. However, the effects of mean horizontal advection upstream and downstream of Maud Rise partially cancel each other when integrating zonally in Fig. 3. Furthermore, horizontal turbulent diffusion, which responds in a similar manner (since it is determined exclusively from observed horizontal temperature gradients, but not the velocity field, and therefore the response to Maud Rise is much smaller), acts to balance the influence of mean horizontal advection upstream of Maud Rise (Fig. 3). Indeed, the overall heat loss that occurs downstream of Maud Rise in Fig. 3 is about 40 W m^{-2}, which is similar to previous estimates in Muench et al. (2001) and also in McPhee et al. (1999; 52 W m^{-2} west of Maud Rise and 23 W m^{-2} over Maud Rise), although these authors focus on the surface heat flux, both using surface drifting buoys.

In Fig. 3, regardless of the perturbation resulting from the influence of Maud Rise, there is a build-up of heat due to mean horizontal advection across the entire southern limb, even if the region over Maud Rise is removed from the integration. There is also a continual removal of heat by horizontal turbulent diffusion regardless of Maud Rise, which would be the case even if we increased the diffusivities on the flanks of Maud Rise, where deep convection has been previously observed (e.g., Akitomo, 2006), since the turbulent diffusion would cancel itself out when integrated zonally across Maud Rise (unless the diffusivities themselves were significantly different on each flank). Thus, it is important that we integrate over large areas and view these results as a representation of the processes influencing large-scale heat distribution of the Weddell Gyre (such as in Section 4.2), and avoid focusing on localised regions. Ultimately, we show that heat flux divergence due to horizontal turbulent diffusion occurs on the flanks of Maud Rise, in agreement with previous studies, which show for instance that baroclinic instabilities on the flanks of Maud Rise are the source of recurrent eddies (Akitomo et al., 2006). Furthermore, Leach et al. (2011) and Ryan et al. (2016) suggest a mixing of WDW with modified recirculating WDW downstream of Maud Rise which would explain the features observed in Fig. 3, where the zonal variation in horizontal turbulent diffusion is smaller west of the Prime Meridian.

Regarding the northern limb of the Weddell Gyre, our findings imply that horizontal turbulent diffusion is a mechanism by which heat enters the region (Fig. 2c). This is in some agreement with Jullion et al. (2014), who use an inverse model based on ship-based sections along 30º E to the coast and also along the northern periphery of the gyre at about 55-60º S in order to diagnose the heat budget of the full water column. They suggest that most of the heat advected into the Weddell Gyre occurs along the northern gyre periphery, rather than from the eastern periphery, and reaches the southwestern Weddell Gyre through recirculation in the interior Weddell Gyre, leading to an entrainment of heat into the Antarctic Slope Front. This analysis is not able to resolve localised features such as the Antarctic Slope Front, but there is an indication, especially from the streamlines, that recirculation of the eastern sub-gyre plays a role in the distribution of heat in the Weddell Gyre (Fig. 1). Furthermore, in Jullion et al. (2014), eddy-induced transport contributes significantly to the heat budget of the Weddell Gyre, with a heat flux of 5 ± 1 TW, out of a net heat flux of 36 ± 13 TW from the ACC into the Weddell gyre, which is primarily due to mean circulation. The results provided in Figs. 2c & 5-7 show agreement with this finding; the Weddell Gyre's northern limb and the IC are dominated by a convergence of heat due to horizontal turbulent diffusion. Both the southern limb and the area directly north of the Weddell Gyre in the ACC, as well as east of ~30°E, in contrast, exhibit heat flux divergence (or cooling) due to horizontal turbulent diffusion (Fig. 2c). This suggests that horizontal turbulent diffusion constitutes an important role in transporting heat into the Weddell Gyre along the open northern boundary as well as from the East- (although large uncertainty in the east requires some caution), in agreement with Jullion et al. (2014). The heat fluxes provided here are somewhat more than the eddy induced heat transport from Jullion et al. (2014) across both the northern and eastern boundary, which, however, accounts for the whole water column, across 2 hydrographic sections which represent the entire open boundary of the Weddell Gyre. We expect their eddy heat flux estimate to exhibit major uncertainties, as it is firstly based on

a station spacing of the temperature and velocity profiles that are not nearly eddy resolving (especially along the northern boundary of the gyre) and secondly represents a one-time snapshot.

According to Tamsitt et al. (2016) and Naveira Garabato et al. (2011), major topographic features result in a divergence of horizontal and vertical eddy heat fluxes, leading to substantial warming in association with regions of enhanced mesoscale energy. Thompson & Salleé (2012) use particle advection experiments to show that the enhancement of eddy kinetic energy occurs downstream off topographic obstacles, which may explain cross-front exchange associated with jets in the lee of topographic features. This may explain the heat flux divergence due to horizontal turbulent diffusion that occurs in the lee of Maud Rise (Fig. 2 and 3). It may also help to explain the fluctuations along the northern limb of the Weddell Gyre in Figs. 2a and 2e, where the topography is complex, creating an open-ocean northern boundary to the Weddell Gyre. Indeed, the alternating bands of convergence and divergence along the northern limb of the gyre between 30° W and 20° E in Figs. 2a and 2e appear to reflect the underlying bathymetry, though the alternating bands are also likely due to the effects of meandering of the northern boundary on a coarse resolution grid.

There is also a relatively strong heat flux divergence due to horizontal turbulent diffusion along the southern boundary of the Weddell Gyre towards the coastline in Fig. 2c, especially between 40 and 10° W, and between Astrid ridge and Gunnerus ridge (between 10 and 30° E), indicating that horizontal turbulent diffusion may also constitute an important role in transporting heat towards the shelves along the southern coastline. Indeed, enhanced diffusive mixing over the continental slope (region not covered by this study) has been observed in the southwestern Weddell Sea (Fer er al., 2016; Daae et al., 2009). We are unable to directly compute turbulent heat fluxes across the southern boundary of the southern inflow limb toward the shelf edge due to the requirement of differencing across grid cells, and caution should be made with any attempt at inferring fluxes due to the large uncertainty of computing the heat budget at the boundary. Yet, we may estimate the shelf-ward heat flux indirectly. Fig. S6b reveals the net diffusive heat flux across the northern boundary of the southern inflow limb to amount to 6.4 ± 0.6 TW. If we subtract this value from the total heat flux divergence due to horizontal turbulent diffusion of the SL of 19 ± 2 TW (Table 3), then we can cautiously infer that most of the remaining horizontal turbulent heat flux occurs southwards towards the ice-covered shelf seas (Fig. 2c), of 12.6 ± 3 TW (southwards having a much larger length with larger negative values in Fig. 2c in comparison to the western end of the SL region, (i.e., the stipled area in Fig. 2b).

These results indicate that horizontal turbulent diffusion may play an important role in transporting heat southwards across the open northern boundary of the Weddell Gyre (Fig. 5b & S6a), and also southwards towards the continental shelves along the Antarctic coast (Fig. 2c). Furthermore, the horizontal turbulent diffusion of heat may allow for the removal of some heat from the southern limb of the Weddell Gyre (Fig. 7b & S6b), before it is able to advect westwards towards the southwestern corner of the gyre, where the fragile large Filchner-Ronne ice shelf and the ice shelves of the Antarctic Peninsula are located (Hellmer et al., 2012), and where recent advance in the understanding of ocean heat fluxes have been made (Ryan et al., 2020). Since the turbulent diffusive heat fluxes are dependent on horizontal temperature gradients (related to geostrophic shear), this implies a complex interaction between the strength of the Weddell Gyre, thus mean horizontal advection, and the rate of meridional turbulent diffusion. Potentially, up to a certain point, meridional turbulent diffusion may provide a buffer, protecting the southwestern gyre from increased advective heat fluxes resulting from an intensified Weddell Gyre, by also increasing in intensity (due to stronger lateral temperature gradients and velocity shear). This mechanism requires careful understanding if we are to understand the role of the Weddell Gyre in the redistribution of heat in a changing climate.

6   Conclusions

Gridded climatologies of temperature and velocity derived from Argo floats spanning 2002-2016 were used to determine the heat budget of a 1000 m thick layer encompassing the core of WDW within the Weddell Gyre. This investigation was to

establish the mechanisms by which heat is distributed throughout the Weddell Gyre, implicitly assuming non-divergent, geostrophic flow conditions. The mechanisms are summarised in the form of a basic schematic in Fig. 8, and interpreted below.
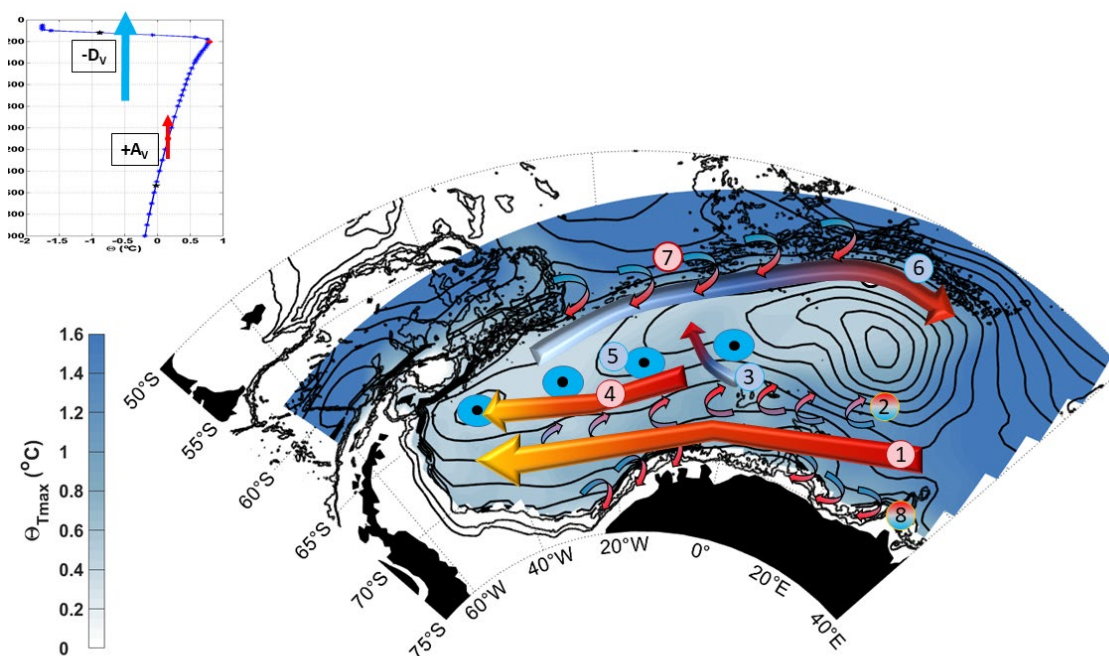
Figure 8: Schematic of proposed mechanisms by which heat is transported throughout the Weddell Gyre, based on interpretation of results in Sections 4 & 5.3.3. The blue-scale colour shading shows Θ_{max} and the black contours show the stream function with 5 Sv spacing, as in Fig. 1. The numbered keys assigned to each feature (arrows and circles) are described in Table 4. Where the colour of the number and feature are red, heat flux convergence (heat source) is indicated, and where they are blue indicates heat flux divergence (heat sink). The horizontal turbulent diffusive fluxes, indicated by small curved arrows (2,7,8), change from blue to red to indicate a direction of heat flux (i.e., in 2, horizontal turbulent diffusion removes heat from the SL northwards into the IC, and southwards to the Antarctic coastline (8), and in 7, removes heat from north of the gyre, into the northern limb of the IC). The change in colour from red to orange of the arrow in the SL (1) and IC-south (4) indicates cooling along the advective pathway as heat is removed from both areas, whereas the change in colour from pale blue to red of the arrow in the northern limb (6) indicates warming of the advective pathway as heat is diffused southwards from across the northern boundary, and to a lesser extent as heat is advected northwards downstream of Maud Rise to circulate the eastern sub-gyre (3). The blue circles with the central black dot (5) demonstrates the upwards loss of heat through the thermocline by vertical turbulent diffusion. The upper left inset shows an example of the vertical temperature profile, with $-D_V$ indicating a vertical diffusion of heat upwards out of the layer through the thermocline, and $+A_V$ indicating a vertical advection of heat upwards into the layer from below.

Table 4: Summary of the key heat budget terms that are shown in the schematic in Fig. 8. The numbers correspond to the number key in Fig. 8, and the associated features in the schematic. Abbreviations used for the heat budget terms are defined in Table 2.

Key	Process	Net heat budget contribution (TW)
1	A_H into SL	+26 ± 4 TW
2	D_H out of SL (into IC-south)	-19.0 ± 2 TW (into IC-south: ~6.4 ± 0.6 TW)
3	A_H out of IC-south (West of MR and East of 10°W; i.e., circulating eastern sub-gyre)	3 ± 3 TW

4	A_H into IC-south (downstream of MR)	5 ± 3 TW
5	D_V out of IC-south	-6 ± 0.3 TW
6	A_H out of IC-north	-68 ± 15 TW
7	D_H into IC-north from ACC	78 ± 4 TW (direct flux across northern boundary is ~32 ± 1 TW, suggesting over half exits the eastern end of the IC-north layer)

If we accept the potential sources of uncertainty discussed in Section 5, we can interpret the results presented in this study as follows:

1. In the SL of the Weddell Gyre, heat *convergence* due to mean horizontal and vertical advection is balanced by a *divergence* of heat due to horizontal and vertical turbulent diffusion. 26±4 TW of heat is advected into the southern limb of the Weddell Gyre (Fig. 8, no. 1), while 19±2 TW of heat is removed from the same region by horizontal turbulent diffusion (Fig. 8, no. 2). 6.4± 0.6 TW of heat is directly removed from the southern limb by horizontal turbulent diffusion northwards into the IC, half of which occurs west of Maud Rise.

2. In contrast, in the IC, heat *convergence* due to horizontal turbulent diffusion is partly balanced by heat *divergence* due to mean horizontal advection. 37±27 TW of heat is advected out of the IC (Fig. 8, no. 6), while 74±9 TW of heat is turbulently diffused into the IC (Fig. 8, no. 7).

3. When we consider the eastward flowing northern limb and the westward flowing southern limb as separate regions, we see that the heat flux *convergence* due to horizontal diffusion mostly occurs in the northern limb of the IC. The net heat flux *convergence* into the IC-north of 78 ± 4 TW is (mainly) due to a southward heat flux across the northern boundary of the gyre (32 ± 1 TW, Fig. 8, no. 7), and also from the eastern gyre periphery. A net heat flux *convergence* due to horizontal turbulent diffusion also occurs in the IC-south of 3.3 ± 1 TW (Fig. 8, no. 2). Horizontal mean advection acts to remove heat from the northern limb of the IC (-68 ± 15 TW; Fig. 8, no. 6).

4. There is an advective pathway of heat northwards from the gyre's southern limb between 10 and 20° W, which has an impact on the spatial distribution of Θ_{max}, and removes 3 ± 3 TW from the IC-south (i.e., north of Maud Rise), between 0°E and 10° W to circulate the eastern sub-gyre (Fig. 8, no. 3). West of 10° W, heat is advected into the IC-south (5 ± 3 TW) (Fig. 8, no. 4). The main mechanism that removes heat from the IC-south is vertical turbulent diffusion (heat is lost upwards through the thermocline with a net flux of -6 ± 0.3 TW; Fig. 8, no. 5).

5. At the southern boundary, there appears to be a diffusive flux of heat towards the shelf seas along the southern coastline, especially between 10 and 30° W, and 10 and 30° E. This may account for the remaining heat flux divergence due to horizontal turbulent diffusion along the southern limb of the Weddell Gyre (i.e., 19 ± 2 TW in table 3, of which 6.4± 0.6 TW is diffused northwards (Fig. 8 and Fig. S6b), leaving a divergence of 12.6 ± 3 TW to be diffused southwards along the southern boundary in Fig. 8, no. 8). While errors are high at the boundary since Argo floats cannot fully resolve shelf edge boundary currents, this may indicate that horizontal turbulent diffusion plays an important role in delivering heat towards the ice-covered shelf seas.

6. In contrast to the horizontal terms, the vertical terms are spatially uniform, where the vertical advection term leads to heat flux convergence throughout both the SL and IC while the vertical turbulent diffusion term results in heat flux divergence. The terms are nearly negligible in comparison to the horizontal terms. Given that Ekman pumping velocity is mostly positive upwards throughout (Fig. S3), and that the lower boundary of the layer is warmer than the

upper boundary throughout (based on the vertical boundary conditions in 2.1, also see example of temperature profile inserted in Fig. 8), we can interpret the vertical terms as:

a. heat is uniformly advected upwards through Ekman upwelling into the layer from below (SL: 0.9±0.3 Wm⁻², or a total of +2.5 ± 0.03 TW, and IC: 0.8±0.2 Wm⁻², or a total of 6.5 ± 0.1 TW).

670

b. heat is diffused upwards out of the top of the layer, due to the relatively strong vertical temperature gradient at the thermocline, and due to vertical instabilities at the thermocline (SL: -2.7 ± 0.5 Wm⁻², or a total or -7.2 ± 0.4 TW, and IC: -2.3 ± 0.3 Wm⁻², or a total of -17 ± 0.6 TW). This heat may eventually be lost to the atmosphere.

7. East of the Prime Meridian, 2 ellipses of strong heat flux divergence and 2 ellipses of strong heat flux convergence

675 are found to the north and south of the eastern sub-gyre respectively. This is directly related to horizontal mean advection and is likely an artifact of a misalignment between horizontal circulation and strong horizontal temperature gradients on a coarse resolution grid. However, the "misalignment" may be linked to the occurrence of unresolved mesoscale eddies that are not represented by turbulent heat flux diffusion, that may be skewing the mean state representation of the temperature and flow fields. This is possibly due to poor data coverage in a region where

680 instabilities are likely generated from the interaction between "cold" regime recirculating WDW and incoming "warm" regime WDW (Gordon and Huber, 1984 and Fig. 1). Unresolved horizontal circulation around Maud Rise adds to the uncertainty in the region. Thus, to improve estimates in the eastern Weddell Gyre, more observations are required to resolve the complex ocean dynamics on smaller length-scales in the eastern sub-gyre region.

685 From using Argo floats, we have described the heat budget of a 1000 m thick layer encompassing the core of WDW within the Weddell Gyre. The role of mean horizontal advection is evident in feeding heat towards the southwestern Weddell Gyre, where the Filchner-Ronne ice shelves and Antarctic Peninsular are located. What is also important, however, is understanding the respective roles of mean horizontal advection and horizontal turbulent diffusion in removing some of that heat from the southern limb of the Weddell Gyre before it is able to reach the southwestern interior. This is crucial since Hellmer et al. (2012)

690 suggest that under future climate scenarios, a redirection of the coastal current toward the Filchner-Ronne ice shelf could lead to increased advection of waters into the ice-shelf cavity, leading to increased basal ice melt from 0.2 to 4 m/year.

Data availability: The Argo float data were collected and made freely available by the International Argo Program and the national programs that contribute to it (http://www.argo.ucsd.edu, http://argo.jcommops.org). The horizontal diffusivities were provided by Florian Sevellec (Sevellec et al., 2020: https://doi.org/10.17882/91335). The ERA5 dataset is available at
695   https://www.ecmwf.int/en/forecasts/datasets/reanalysis-datasets/era5. Sea-ice data are available at https://nsidc.org/data/nsidc-0116/versions/4. Objectively mapped temperature from Reeve et al. (2016) is available at https://doi.pangaea.de/10.1594/PANGAEA.842876.

Author Contribution: K.A. Reeve performed the data analysis, figure preparation and wrote the manuscript with contributions from all authors.

700   **Competing interests**: The authors declare that they have no conflict of interest.

Acknowledgements: These data were collected and made freely available by the International Argo Program and the national programs that contribute to it (http://www.argo.ucsd.edu, http://argo.jcommops.org). The Argo Program is part of the Global Ocean Observing System. The GEBCO Digital Atlas is published by the British Oceanographic Data Centre on behalf of IOC and IHO, 2003. The mean velocities derived from mooring data were provided by Nicolas Le Paih, to whom the authors are
705   indebted to. The horizontal diffusivities were provided by Florian Sevellec (Sevellec et al., 2020). KR is supported through the grant 424330345 of the Deutsche Forschungsgemeinschaft within the framework of SPP 1158 Antarktisforschung. The study also makes a contribution to EU SO-CHIC programme (grant number 821001) through the involvement of TK. This study is a contribution to the project T3 of the Collaborative Research Centre TRR 181 "Energy Transfers in Atmosphere and Ocean" funded by the Deutsche Forschungsgemeinschaft (DFG, German Research Foundation; project no. 274762653). MV
710   was funded by the BMBF project APEAR (#03V01461).

7   References

Akitomo, K.: Thermobaric deep convection, baroclinic instability, and their roles in vertical heat transport around Maud Rise in the Weddell Sea, J. Geophys. Res., 111, C09027, doi:10.1029/2005JC003284, 2006.

715   Argo: Argo float data and metadata from Global Data Assembly Centre (Argo GDAC). SEANOE. https://doi.org/10.17882/42182, 2000.

Behrendt, A., Fahrbach, E., Hoppema, M., Rohardt, G., Boebel, O., Klatt, O., Wisotzki, A., and Witte, H.: Variations of winter water properties and sea ice along the Greenwich Meridian on decadal time scales, Deep-Sea Research Part II, 58, 2524–2532, doi:10.1016/j.dsr2.2011.07.001, 2011.

720   Brown, P.J., Jullion, L., Landschützer, P., Bakker, D.C., Naveira Garabato, A.C., Meredith, M.P., Torres-Valdés, S., Watson, A.J., Hoppema, M., Loose, B. and Jones, E.M.: Carbon dynamics of the Weddell Gyre, Southern Ocean. Global Biogeochemical Cycles, 29(3), pp.288-306, 2015.

Cisewski, B., Strass, V.H., and Prandke, H.: Upper-ocean vertical mixing in the Antarctic Polar Front Zone, Deep-Sea Research II, 52:1087–1108. doi:10.1016/j.dsr2.2005.01.010, 2005.

725   Cisewski, B., V. H. Strass, M. Losch, and Prandke, H.: Mixed layer analysis of a mesoscale eddy in the Antarctic Polar Front Zone, J. Geophys. Res., 113, C05017, doi: 10.1029/2007JC004372, 2008.

Cisewski, B., Strass, V. and Leach, H.: Circulation and transport of water masses in the Lazarev Sea, Antarctica, during summer and winter 2006, Deep Sea Res. I, 58, pp. 186-199, doi:10.1016/j.dsr.2010.12.001, 2011.

Cole, S. T., C. Wortham, E. Kunze, and Owens, W. B.: Eddy stirring and horizontal diffusivity from Argo float observations: Geographic and depth variability. Geophys. Res. Lett., 42, 3989–3997. doi: 10.1002/2015GL063827, 2015.

Daae, K.L., Fer, I. and Abrahamsen, E.P.: Mixing on the continental slope of the southern Weddell Sea. J. Geophys. Res.: Oceans, 114(C9), 2009.

745   Deacon, G.: The Weddell Gyre. Deep-Sea Res. I, 26A, 981–995, 1979.

Donnelly, M., Leach, H. and Strass, V.: Modification of the deep salinity-maximum in the Southern Ocean by circulation in the Antarctic Circumpolar Current and the Weddell Gyre. Ocean Dynamics, 67(7), pp.813-838, 2017.

Fahrbach, E., Hoppema, M., Rohardt, G., Schröder, M., and Wisotzki, A.: Decadal-scale variations of water mass properties in the deep weddell sea, Ocean Dynamics, 54, 77-91, 10.1007/s10236-003-0082-3, 2004.

750   Fahrbach, E., Hoppema, M., Rohardt, G., Boebel, O., Klatt, O., and Wisotzki, A.: Warming of deep and abyssal water masses along the greenwich meridian on decadal time scales: The weddell gyre as a heat buffer, Deep Sea Res. Part II: Topical Studies in Oceanography, 58, 2509-2523, http://dx.doi.org/10.1016/j.dsr2.2011.06.007, 2011.

Forryan, A., Martin, A.P., Srokosz, M.A., Popova, E.E., Painter, S.C. and Renner, A.H.: A new observationally motivated Richardson number based mixing parametrization for oceanic mesoscale flow. J. Geophys. Res.: Oceans, 118(3), pp.1405-
755   1419, 2013.

Foster, T. D., Foldvik, A., and Middleton, J. H.: Mixing and bottom water formation in the shelf break region of the southern weddell sea, Deep Sea Res. Part A. Oceanographic Research Papers, 34, 1771-1794, http://dx.doi.org/10.1016/0198-0149(87)90053-7, 1987.

Gordon, A.L., Huber, B.A.: Thermohaline stratification below the Southern Ocean sea ice. J.Geophys Res., 89 (C1), 641–648,
760   1984.

Gouretski, V.V., and Danilov, A.I.: Weddell Gyre: structure of the eastern boundary. Deep-Sea Res. I, 40:561–582. doi:10.1016/0967-0637(93)90146-T, 1993.

Hellmer, H., Kauker, F., Timmermann, R., Determann, J., and Rae, J.: Twenty-first-century warming of a large Antarctic ice-shelf cavity by a redirected coastal current. Nature. 485. 225-8. 10.1038/nature11064, 2012.

765   Hersbach, H., Bell, B., Berrisford, P., et al.: The ERA5 global reanalysis. Q J R Meteorol Soc. 146: 1999– 2049. https://doi.org/10.1002/qj.3803, 2020.

IOC, IHO, and BODC: Centenary edition of the gebco digital atlas, in: Published on CD-ROM on behalf of the Intergovernmental Oceanographic Commission and the International Hydrographic Organization as part of the General Bathymetric Chart of the Oceans, British Oceanographic Data Centre, Liverpool, UK, 2003.

770   Jones, R. W., I. A. Renfrew, A. Orr, B. G. M. Webber, D. M. Holland, and Lazzara, M. A.: Evaluation of four global reanalysis products using in situ observations in the Amundsen Sea Embayment, Antarctica, J. Geophys. Res., Atmosphere, 121, 6240–6257, doi: 10.1002/2015JD024680, 2016.

Jullion, L., Garabato, A.C.N., Bacon, S., Meredith, M.P., Brown, P.J., Torres-Valdés, S., Speer, K.G., Holland, P.R., Dong, J., Bakker, D. and Hoppema, M.: The contribution of the Weddell Gyre to the lower limb of the Global Overturning Circulation. J.
775   Geophys. Res.: Oceans, 119(6), pp.3357-3377, 2014.

Kerr, R., Dotto, T.S., Mata, M.M., Hellmer, H.H.: Three decades of deep water mass investigation in the Weddell Sea (1984-2014): Temporal variability and changes, Deep-Sea Res. Part II, https://doi.org/10.1016/j.dsr2.2017.12.002, 2017.

Klatt, O., Fahrbach, E., Hoppema, M., and Rohardt, G.: The transport of the weddell gyre across the prime meridian, Deep Sea Res. Part II: Topical Studies in Oceanography, 52, 513-528, http://dx.doi.org/10.1016/j.dsr2.2004.12.015, 2005.

780   Leach, H., Strass, V. and Cisewski, B.: Modification by Lateral Mixing of the Warm Deep Water entering the Weddell Sea in the Maud Rise Region, Ocean Dynamics, 61 (1), pp. 51-68, doi:10.1007/s10236-010-0342-y, 2011.

Ledwell, J.R., Watson, A.J., and Law, C.S.: Mixing of a tracer in the pycnocline. J. Geophys Res.-Oceans, 103:21499– 21529, 1998.

Ledwell, J.R., Montgomery, E.T., Polzin, K.L., St Laurent, L.C., Schmitt, R.W., and Toole, J.M.: Evidence for enhanced
785   mixing over rough topography in the abyssal ocean, Nature 403:179–182, 2000.

McDougall T. J. and Barker, P. M.: Getting started with TEOS-10 and the Gibbs Seawater (GSW) Oceanographic Toolbox, 28 pp., SCOR/IAPSO WG127, ISBN 978-0-646-55621-5, 2011.

Menemenlis, D., Fukumori, I., and Lee, T.: Using Green's Functions to calibrate and Ocean General Circulation Model, Monthly Weather Review, 133, 1224–1240, 2005.

790   Menemenlis, D., Campin, J.M., Heimbach, P., Hill, C., Lee, T., Nguyen, A., Schodlok, M., and Zhang, H.: ECCO2: High resolution global ocean and sea ice data synthesis, Mercator Ocean Quarterly Newsletter, 31, 13–21, 2008.

Meredith, M.P., Gordon, A.L., Naveira Garabato, A.C., Abrahamsen, E.P., Huber, B.A., Jullion, L., and Venables, H.J.: Synchronous intensification and warming of Antarctic Bottom Water outflow from the Weddell Gyre, Geophys. Res. Lett., 38, L03603, doi:10.1029/2010GL046265, 2011.

795   Muench, R. D., Morison, J. H., Padman, L., Martinson, D., Schlosser, P., Huber, B., and Hohmann, R.: Maud Rise revisited, J. Geophys. Res., 106, 2423–2440, 2001.

Naveira Garabato, A.C., McDonagh, E.L., Stevens, D.P., Heywood, K.J. and Sanders, R.J.: On the export of Antarctic Bottom Water from the Weddell Sea, Deep-Sea Res. Part II-Topical Studies in Oceanography, 49(21), pp. 4715-4742, 2002.

Naveira Garabato, A.C., Oliver, K.I.C., Watson, A.J. and Messias, M.J.: Turbulent diapycnal mixing in the Nordic Seas, J. Geophys. Res., 109:C12010, 9 pp. doi: 10.1029/2004JC002411, 2004a.

Naveira Garabato, A.C., Polzin, K.L., King, B.A., Heywood, K.J., and Visbeck, M.: Widespread intense turbulent mixing in the Southern Ocean, Science 303:210–213. doi: 10.1126/science.1090929, 2004b.

Naveira Garabato, A.C., Stevens, D.P., Watson, A.J., and Roether, W.: Short-circuiting of the overturning circulation in the Antarctic circumpolar current, Nature, 447:194–197. doi: 10.1038/nature05832, 2007.

Naveira Garabato, A.C., Ferrari, R., and Polzin, K.L.: Eddy stirring in the Southern Ocean. J.Geophys. Res.: Oceans 116: C09019. doi:10.1029/2010jc006818, 2011.

Naveira Garabato, A.C., Zika, J.D., Jullion, L., Brown, P.J., Holland, P.R., Meredith, M.P., and Bacon, S.: The thermodynamic balance of the Weddell Gyre, Geophys. Res. Lett., 43, 317–325, doi:10.1002/2015GL066658, 2016.

Okubo, A.: Oceanic diffusion diagrams. Deep Sea Res. and Oceanographic Abstracts, 18:789–802. doi:10.1016/0011-7471(71) 90046-5, 1971.

Orsi, A.H., Nowlin, W.D. Jr, and Whitworth, T. III: On the circulation and stratification of the Weddell gyre, Deep-Sea Res. I, 40:169–203. doi:10.1016/0967-0637(93)90060-G, 1993.

Orsi, A.H., Whitworth, T. III, and Nowlin, W.D. Jr: On the meridional extent and fronts of the Antarctic circumpolar current. Deep-Sea Res. I, 42:641–673. doi:10.1016/0967-0637(95) 00021-W, 1995.

Park, J. J., Kim, K., King, B. A. and Riser, S. C.: An Advanced Method to Estimate Deep Currents from Profiling Floats, J. Atmospheric and Oceanic Technology, 22(8), pp. 1294-1304, 2005.

Polzin, K.L., Toole, J.M., Ledwell, J.R., and Schmitt, R.W.: Spatial variability of turbulent mixing in the abyssal ocean. Science 276:93–96. doi:10. 1126/science.276.5309.93, 1997.

Reeve, K. A., Boebel, O., Kanzow, T., Strass, V., Rohardt, G. and Fahrbach, E.: A gridded data set of upper-ocean hydrographic properties in the Weddell Gyre obtained by objective mapping of Argo float measurements, Earth Syst. Sci. Data, 8(1), pp. 15-40, 2016.

Reeve, K. A., Boebel, O., Strass, V., Kanzow, T., Gerdes, R.: Horizontal Circulation and volume transports in the Weddell Gyre derived from Argo float data, Progress in Oceanography, 175, pp. 263-283, https://doi.org/10.1016/j.pocean.2019.04.006, 2019.

Rhein, M., Rintoul, S.R., Aoki, S., Campos, E., Chambers, D., Feely, R.A., Gulev, S., Johnson, G.C., Josey, S.A., Kostianoy, A., Mauritzen, C., Roemmich, D., Talley, L.D. and Wang, F.: Observations: Ocean. In: Climate Change 2013: The Physical Science Basis. Contribution of Working Group I to the Fifth Assessment Report of the Intergovernmental Panel on Climate Change [Stocker, T.F., Qin, D., Plattner, G.-K., Tignor, M., Allen, S.K., Boschung, J., Nauels, A., Xia, Y., Bex, V. and Midgley, P.M. (eds.)]. Cambridge University Press, Cambridge, United Kingdom and New York, NY, USA, 2013.

Roemmich, D., Gilson, J., Willis, J., Sutton, P., and Ridgway, K.: Closing the Time-Varying Mass and Heat Budgets for Large Ocean Areas: The Tasman Box. J. Climate, 18, 2330–2343, https://doi.org/10.1175/JCLI3409.1, 2005.

Ryan, S., Hellmer, H. H., Janout, M., Darelius, E., Vignes, L., & Schröder, M.: Exceptionally warm and prolonged flow of Warm Deep Water toward the Filchner-Ronne Ice Shelf in 2017. Geophys. Res. Lett., 47, e2020GL088119. https://doi.org/10.1029/2020GL088119, 2020.

Ryan, S., Schröder, M., Huhn, O., and Timmermann, R.: On the warm inflow at the eastern boundary of the Weddell Gyre, Deep-Sea Res. I, 107, 70-81, https://doi.org/10.1016/j.dsr.2015.11.002, 2016.

Schlosser, P., Roether, W. and Rohardt, G.: Helium-3 balance of the upper layers of the northwestern Weddell Sea. Deep Sea Res. Part A. Oceanographic Research Papers, 34(3), pp.365-377, 1987.

Schröder, M. and Fahrbach, E.: On the structure and the transport of the eastern Weddell Gyre. Deep Sea Res. Part II: Topical Studies in Oceanography, 46(1-2), pp.501-527, 1999.

Sévellec F., Verdière A.C. d., Kolodziejczyk N.: Deep Horizontal Turbulent Diffusivity. SEANOE. https://doi.org/10.17882/91335, 2020.

845 Sévellec, F., Verdière, A. C. d., & Kolodziejczyk, N. Estimation of Horizontal Turbulent Diffusivity from Deep Argo Float Displacements, J. Physical Oceanography, 52(7), 1509-1529, 2022.

Sonnewald, M., Reeve, KA., Lguensat, R.: The Southern Ocean supergyre: a unifying dynamical framework identified by machine learning. Science Advances, IN REVIEW.

Strass, V.H., Rohardt, G., Kanzow, T., Hoppema, M. and Boebel, O.: Multidecadal warming and density loss in the deep Weddell Sea, Antarctica. J. Climate, 33(22), pp.9863-9881, 2020.

850 Tamsitt, V., Talley, L.D., Mazloff, M.R., and Cerovecki, I.: Zonal Variations in the Southern Ocean heat budget, J. Climate, 29, 6563-6579, doi:10.1175/JCLI-D-15-0630.1, 2016.

Thompson, A., Salleé, J.B.: Jets and topography: Jet transitions and the impact on transport in the Antarctic Circumpolar Current, J. Physical Oceanography, 42, 956-972, 2012.

Tschudi, M., Meier, W. N., Stewart, J. S., Fowler, C., and Maslanik, J.: Polar Pathfinder Daily 25 km EASE-Grid Sea Ice
855 Motion Vectors, Version 4. Boulder, Colorado USA. NASA National Snow and Ice Data Center Distributed Active Archive Center. https://doi.org/10.5067/INAWUWO7QH7B, 2019.

Zika, J.D., Sloyan, B.M. and McDougall, T.J: Diagnosing the Southern Ocean overturning from tracer fields. J. Physical Oceanography, 39(11), pp.2926-2940, 2009.